Determination of the multiple-scattering correction factor and its cross-sensitivity to scattering and wavelength dependence for different AE33 Aethalometer filter tapes: A multi-instrumental approach

Jesús Yus-Díez[1,2], Vera Bernardoni[3], Griša Močnik[4,5], Andrés Alastuey[1], Davide Ciniglia[3], Matic Ivančič[6], Xavier Querol[1], Noemí Perez[1], Cristina Reche[1], Martin Rigler[6], Roberta Vecchi[3], Sara Valentini[3], and Marco Pandolfi[1]

[1]Institute of Environmental Assessment and Water Research (IDAEA-CSIC), C/Jordi Girona 18-26, 08034, Barcelona, Spain
[2]Grup de Meteorologia, Departament de Física Aplicada, Universitat de Barcelona, C/Martí i Franquès, 1, 08028, Barcelona, Spain
[3]Dipartimento di Fisica "A. Pontremoli", Università degli Studi di Milano & INFN-Milan, via Celoria 16, 20133 Milano, Italy
[4]Center for Atmospheric Research, University of Nova Gorica, Vipavska 11c, SI-5270 Ajdovščina, Slovenia.
[5]Department of Condensed Matter Physics, Jozef Stefan Institute, Jamova 39, SI-1000 Ljubljana, Slovenia
[6]Aerosol d.o.o., Ljubljana, Slovenia
Correspondence: jesus.yus@idaea.csic.es

Abstract.

~~Accurate measurements of light absorption by aerosolized particles , especially black carbon (BC), are~~ Providing reliable observations of aerosol particles absorption properties at spatial and temporal resolutions suited to climate models is of utter importance ~~since BC represents the second most important climate-warming agent after carbon dioxide (CO$_2$). Reducing the~~

5 ~~uncertainties related to the absorption measurement techniques will improve the global estimation of BC concentration and the radiative effects of light absorbing aerosols. Currently~~ to better understand the effects that atmospheric particles have on climate. Nowadays, one of the instruments most widely used ~~instruments for BC and absorption measurements is the~~ in international monitoring networks for in-situ surface measurements of light absorption properties of atmospheric aerosol particles is the ~~multi-wavelength~~ dual-spot aethalometer, AE33~~, which~~. The AE33 derives the absorption coefficients of aerosol particles

10 at 7 different wavelengths from the measurements of ~~optical attenuation~~ the optical attenuation of light through a filter where particles are continuously collected. An accurate determination of the absorption ~~coefficient~~ coefficients from AE33 instrument relies on the quantification of the non-linear processes related to the ~~collection of sample~~ sample collection on the filter. The multiple-scattering correction factor (C~~(λ)~~), which depends on the filter tape used and on the optical properties of the collected particles, is the parameter with both the greatest uncertainty and the greatest impact on the absorption coefficients derived from

15 the AE33 measurements.

~~An~~ Here we present an in-depth analysis of the AE33 multiple-scattering correction factor C and its wavelength dependence for ~~different~~ two different and widely used filter tapes, ~~i.e. the old~~most referenced ~~known as~~ namely: the old, and most referenced, TFE-coated glass~~and the current~~, or M8020, filter tape and the currently, and most widely used~~M8060, has been~~

~~carried out by comparing the AE33 attenuation measurements~~ M8060 filter tape. For performing this analysis, we compared

the attenuation measurements from AE33 with the absorption ~~measurements from~~ coefficients measured with different filter-based techniques. Online co-located multi-angle absorption photometer (MAAP) measurements and offline PP_UniMI polar photometer measurements were ~~used with this aim. We~~ employed as reference absorption measurements for this work. To this aim, we used data from three different measurement stations located in North-East of Spain, namely: an urban background station (Barcelona; BCN), a regional background station (Montseny; MSY) and a mountain-top station (Montsec d'Ares; MSA). The median C values (at 637 nm) measured at the three stations ranged between 2.29 (at BCN and MSY; lowest 5th percentile of 1.97 and highest 95th percentile of 2.68) and 2.51 (at MSA; lowest 5th percentile of 2.06 and highest 95th percentile of 3.06). The ~~C factor was wavelength-dependent only at the mountain-top station, whereas at the urban and regional stations no statistically significant difference was found at the 7 different AE33 wavelengths. The wavelength-dependence of C at the mountain station was in part driven by the predominant effect of dust particles during Saharan dust outbreaks at this station.~~

~~At the mountain station, neglecting the wavelength dependence of the C factor led to an underestimation of the Absorption Ångström Exponent (AAE) of 12%. The~~ analysis of the cross-sensitivity to scattering ~~for different filter tapes~~, for the two filter tapes considered here, revealed a large increase of the C factor ~~at the three stations~~ when the single scattering albedo (SSA) of the collected particles was above ~~0.90-0.95, with~~ a given threshold, up to a 3-fold increase above the average C values. The ~~result~~ SSA threshold appeared to be site-dependent, and ranged between 0.90 to 0.95 for the stations considered in the study. The results of the cross-sensitivity to scattering displayed a fitted constant multiple scattering parameter, C_f, of 2.21 and 1.96, and a cross-sensitivity factor, m_s, of ~~0.8% and 1.7%~~ 1.8% and 3.4% for MSY and MSA stations, respectively, for the TFE-coated glass filter tape. For the M8060 filter tape, C_f of 2.50, 1.96, 1.82 and ~~a~~ m_s of ~~0.7%, 1.5%, 2.7%~~ 1.6%, 3.0%, 4.9%, for BCN, MSY and MSA stations, respectively, were obtained. SSA variations also influenced the spectral dependence of the C, which showed an increase with wavelength when SSA was above the site-dependent threshold. Below the SSA threshold, no statistically significant dependence of the C with wavelength was observed. For the measurement stations considered here, the wavelength-dependence of C was to some extent driven by the presence of dust particles during Saharan dust outbreaks that had the potential to increase the SSA above the average values. At the mountain-top station, an omission of the wavelength dependence of the C factor led to an underestimation of the Absorption Ångström Exponent (AAE) up to a 12%. Differences in the absorption coefficient determined from AE33 measurements at BCN, MSY and MSA of around a 35-40 % can be expected when using the site-dependent C ~~determined experimentally~~ experimentally obtained instead of the nominal C value. Due to the fundamental role that the SSA of the particles collected on the filter tape has on the multiple scattering parameter C, we present a methodology that allows to recognize the conditions upon which the use of a constant and wavelength independent C is feasible.

1 Introduction

Atmospheric aerosol particles play an important role on the Earth's radiative balance directly by scattering and absorbing solar and terrestrial radiation and indirectly by acting as cloud condensation nuclei. Large uncertainties still exist on the effects that

atmospheric particles have on climate (Myhre et al., 2013). In fact, the aerosol-radiation interaction depends on aerosol properties such as aerosol size distribution, mixing state, and refractive index, among others (e.g. Bond et al., 2013). ~~Furthermore, no standard reference material currently exists for instrument calibration to determine the aerosol particles optical properties.~~

55 Globally, aerosols have helped to reduce the warming effect from greenhouse gases because of their net cooling effect on climate (Myhre et al., 2013). However, this influence is likely to be reduced over the coming decades as air pollution measures are implemented around the world (Samset et al., 2018), as it is already the case in parts of Europe and North America (Collaud Coen et al., 2020). Therefore, in order to properly constrain global models, it is necessary to better characterize the atmospheric absorption by aerosols from observations. Among the atmospheric aerosols, black carbon (BC) ~~,~~ stands out as

60 phenomenologically different, being the most efficient light absorbing aerosol component and being responsible for the second most important contribution to positive climate forcing after carbon dioxide (Myhre et al., 2013). However, there are still large uncertainties related to the radiative forcing of BC particles. In fact, the climate forcing potential of BC is influenced by BC properties which are strongly source and site dependent ~~(Houghton, 2001; Kirchstetter et al., 2004a; Ramanathan and Carmichael, 2008; M~~ In addition to BC, atmospheric absorption by aerosol particles is also driven by specific organic compounds (e.g. from incom-

65 plete combustion, biomass smoldering, and secondary and biogenic sources) often referred to as Brown Carbon (BrC) and by mineral dust (e.g. Alfaro et al., 2004). Unlike BC, which absorbs radiation in a wide range of wavelengths (from UV to infrared) with a wavelength independent refractive index, BrC and mineral dust refractive index increases at shorter wavelengths, close to the UV range (Kirchstetter et al., 2004b; Andreae and Gelencsér, 2006; Bergstrom et al., 2007; Laskin et al., 2015; Cappa et al., 2019). Therefore, having at disposal accurate absorption measurement techniques is crucial to determine particles light

70 absorption which can afterwards be used in climate projections (Mengis and Matthews, 2020; Wang et al., 2020). Moreover, there is also the need of standard aerosol particles to use as reference for quality assurance of absorption measurements, such as the recently developed flame-generated soot in Ess and Vasilatou (2019).

There are three main approaches in the literature to determine aerosol particles light absorption: by measuring the suspended particles in a cell, e.g. with photo-thermal interferometry or photo-acoustic techniques, and by either on-line or off-line filter-

75 based photometer methods (e.g., Lin et al., 1973; Terhune and Anderson, 1977; Hansen et al., 1984; Stephens et al., 2003; Moosmüller et al., 2009; Ajtai et al., 2010; Vecchi et al., 2014). Among the indirect methods for measuring absorption, the "subtraction method", which does not rely on a filter, calculates the absorption from the difference between extinction and scattering by suspended particles (Singh et al., 2014). However, this method can lead to large errors at large single scattering albedo (SSA) values when the extinction is dominated by scattering (Onasch et al., 2015). On-line measurement methodologies

80 based on particle suspension, such as the photo-acoustic spectroscopy (PAS) (Ajtai et al., 2010), have the advantage of measuring directly the absorption by particles suspended in a sampling cell avoiding filter-based artifacts. However, in the case of photo-acoustic spectroscopy measurements, the heating of the sample and the evaporation of coating materials on the sample may lead to higher detection limit and artifacts impairing the measurement accuracy (Lack et al., 2006; Linke et al., 2016). The photo-thermal interferometry (PTI) is an absorption measurement technique originally developed for measurements of

85 trace gases that has also been applied to aerosol measurements (Lee and Moosmüller, 2020; Visser et al., 2020). However, the aforementioned techniques have so far proved difficult to deploy in a field setting thus limiting their broader use in international

measurements networks. Filter-based instruments (either on-line or off-line) rely on the sampling of aerosol particles collected in a filter matrix and on the measurement ~~, with a photometer,~~ of the resulting change of light intensity with a photometer, either on the transmittance (Hansen et al., 1984; Bond et al., 1999; Drinovec et al., 2015), or on both transmittance and reflectance (Petzold and Schönlinner, 2004). This method is affected by artifacts resulting mainly from the effects that the filter has on the measurements. Off-line in-house made filter based polar photometers, which measure both transmittance and reflectance, are deployed at some research centers. Examples are the MWAA (multi-wavelength absorption analyzer) deployed at University of Genoa (Massabò et al., 2013) and the PP_UniMI polar photometer deployed at University of Milan (Vecchi et al., 2014; Bernardoni et al., 2017). These methods can perform accurate absorption measurements by increasing the number of measuring angles (Massabò et al., 2013; Vecchi et al., 2014; Bernardoni et al., 2017) thus allowing an accurate determination of the filter artifacts.

The main advantage of the on-line filter-based methods is that these techniques are ease of use, allow for unattended operation, are relatively inexpensive and provide real-time data. For these reasons, these methods are widely used in international networks such as the Global Atmosphere Watch (GAW, World Meteorological Organization) and the European Research Infrastructure for the Observation of Aerosol, Clouds and Trace Gases (ACTRIS; ~~www.actris.eu~~www.actris.eu). The most used filter-based instruments are the Aethalometer (Hansen et al., 1984; Drinovec et al., 2015), the Particle Soot Absorption Photometer (PSAP, Bond et al., 1999), the Continuous Light Absorption Photometer ~~(CLAP; Ogren et al., 2017)~~(CLAP; Ogren et al., 2017), and the Multi-Angle Absorption Photometer (MAAP, Model 5012, Thermo, Inc., USA; Petzold and Schönlinner, 2004). The measured mass concentration of light absorbing carbonaceous aerosol inferred via optical attenuation of light is referred to as equivalent BC (eBC; Petzold et al., 2013). The main artifacts affecting the light absorption measurements of these instruments are the multiple light scattering within the filter, the filter loading effect and the particle scattering correction (Liousse et al., 1993; Bond et al., 1999; Weingartner et al., 2003; Schmid et al., 2006; Collaud Coen et al., 2010; Lack et al., 2014). Algorithms for correcting these artifacts have been applied and their efficacy tested over the years (Weingartner et al., 2003; Arnott et al., 2005; Schmid et al., 2006; Virkkula et al., 2007; Collaud Coen et al., 2010; Virkkula et al., 2015). Currently, due to the described limitations of the filter-based photometers and other in-situ methods, no reference technique for measuring near-real time aerosol particles light absorption is available (Petzold et al., 2013; Lack et al., 2014).

The filter loading effect consists in the accumulation of particles and the consequent loss of sensitivity of the instrument with an increasing particle load (Bond et al., 1999; Weingartner et al., 2003; Lack et al., 2008; Moosmüller et al., 2009). The cross-sensitivity to scattering is the consequence of the multiple light scattering within the filter fibers and between particles and fibers, thus it is largely dependent on the single scattering albedo of the deposited aerosols. For the older Aethalometer model (AE31) the filter loading effect has been thoroughly studied and different methods for its quantification have been suggested. These methods use for example the discontinuity between the eBC concentration measurements before and after a filter spot is changed (Weingartner et al., 2003; Virkkula et al., 2007), or use the relationship between the eBC concentration and light attenuation (Park et al., 2010; Segura et al., 2014; Drinovec et al., 2015) to correct for filter loading effect. For the AE33 model the loading effect is corrected on-line using the dual-spot technology (Drinovec et al., 2015). In addition, the different physical and chemical properties of the collected particles influence particle optical properties, such as the backscatter fraction and

the single scattering albedo (SSA), thus affecting also the multiple scattering of the collected particles and the filter loading effect (Weingartner et al., 2003; Lack et al., 2008; Virkkula et al., 2015; Drinovec et al., 2017). Among the on-line filter-based instruments, the Multi Angle Absorption Photometer (MAAP) ~~uses also~~ also uses the measurements of light scattered

125   by the blank and loaded filter in order to take into account ~~for~~ both the loading effect and the aerosol particles multiple scattering. Consequently, the MAAP directly provides particle absorption coefficients similar to those obtained with other types of instruments (e.g. PAS; Petzold and Schönlinner, 2004; Petzold et al., 2005).

~~Currently, due to the described limitations of the filter-based photometers and other in-situ methods, no reference technique for measuring aerosol particles light absorption is available (Petzold et al., 2013; Lack et al., 2014). In the~~ The multi-wavelength

130   dual-spot Aethalometer software (AE33, Magee Scientific, Aerosol d.o.o. - Drinovec et al., 2015) corrects the loading effect ~~is corrected~~ on-line and ~~, furthermore, the AE33 software~~ directly implements the use of a correction factor (C) related to the multiple scattering within the filter matrix to convert the measured attenuation to an absorption coefficient. This C factor is generally assumed ~~a-priori~~ a priori, but it can be experimentally determined by using independent absorption measurements or by comparisons with other filter photometers(e.g. Weingartner et al., 2003; Arnott et al., 2005; Drinovec et al., 2015; Backman et al.,

135   2017). For previous filter tapes and aethalometer versions different values of the multiple scattering parameter have been reported: for the AE31 quartz filter Weingartner et al. (2003) proposed a value of 2.14 which later on was recommended to be 3.5, i.e. larger by a factor of 1.64 (Müller, 2015; WMO, 2016); for the AE33 Drinovec et al. (2015) found a C of 1.57 for the Pallflex Teflon-coated glass fiber (TFE-coated glass, also known as M8020), which, after re-normalization using the factor 1.64, resulted in C=2.57. Moreover, different experimental C factor values have been obtained ranging between 2.57-4.24 (Müller et al.,

140   2011b; Drinovec et al., 2020; Laing et al., 2020; Valentini et al., 2020a; Bernardoni et al., 2020). In addition, ~~these filters~~ the quartz filter for the AE31 and the TFE-coated glass filter for the AE33 have been found to feature a cross-sensitivity to scattering, m_s, ranging between 1 and ~~5~~3% ~~(Müller, 2015; Drinovec et al., 2015; Zhang et al., 2018; Corbin et al., 2018; Laing et al., 2020; Drino To~~ (Müller et al., 2011a; Müller, 2015; Drinovec et al., 2015; Zhang et al., 2018; Corbin et al., 2018; Laing et al., 2020; Drinovec et al., 20 However, to the best of our knowledge, so far, no in-situ ambient measurements have been ~~reported in literature for~~ used for

145   a detailed characterization of the recommended new M8060 filter tape ~~and~~. Moreover, no sensitivity studies of the cross-sensitivity to scattering of the C factor have been ~~carried out for this new filter tape either~~ reported and only very few studies dealt with the wavelength dependence of the C for either the previous and the current filter tapes.

The recent comparison between the MAAP and the off-line PP_UniMI polar photometer carried out by Valentini et al. (2020b) pointed to a possible measurement bias of the MAAP absorption coefficients. It is well established that the MAAP,

150   although limited to one measuring wavelength, is the most accurate filter-based on-line method available for the determination of the absorption coefficient (Petzold et al., 2005; Sheridan et al., 2005; Andreae and Gelencsér, 2006; Müller et al., 2011a). Therefore, it is often taken as the reference in inter-comparison exercises with other instruments, such as the AE33 e.g. in Backman et al. (2017). The discrepancy between MAAP and PP_UniMI reported by Valentini et al. (2020b) was mainly attributed to the value of the fraction of backscattered radiation set in the MAAP algorithm and directly measured by PP_UniMI

155   ~~thanks to the~~ due to its high angular resolution which scans the whole scattering plane (resolution of 0.4 degrees in the scattering

angle range 0-173°). Valentini et al. (2020b) also reported no differences between MAAP and PP_UniMI when the PP_UniMI was used with the same assumptions as those used in the MAAP (PaM as defined in Valentini et al., 2020b).

The main ~~aim~~ objective of this study is to characterize the C factor for different filter tapes used in AE33 instruments including the currently used M8060. To ~~do this~~ this aim, we compared the absorption coefficient measurements from the off-line

160   PP_UniMI polar photometer with the on-line MAAP and AE33 measurements performed at three measurement stations (urban background, ~~regional background~~ BCN; regional background, MSY; and mountain-top~~stations~~, MSA) in the Western Mediterranean Basin (WMB). ~~As mentioned, the comparison between PP_UniMI and MAAP was reported in Valentini et al. (2020b) where data from BCN and MSY stations were also used to evaluate the performances of PP_UniMI vs MAAP. One of the objectives of this study is using the multi-wavelength absorption coefficient measurements from the off-line polar photometer extrapolated to~~

165   ~~the seven AE33 measurement wavelengths to study the wavelength dependence of the AE33 C factor at the three measurement sites. Moreover, the~~ The novelty of this study relies ~~also in the fact that we studied the seasonal variations~~ in the the seasonal and diel variations analysis of the C factor~~and explored its~~, and especially, in the exploration of the cross-sensitivity to scattering ~~relating it to the physical and~~ of C and its relationship with the intensive optical properties of the collected particles at the three sites. This analysis allowed us to obtain both the multiple scattering parameter, C_f, and the cross-sensitivity to

170   scattering, m_s, constants for the M8060 filter currently used by the AE33 aethalometers. Moreover, we compared the results for the M8060 filter tape with the previously used TFE-coated glass filter tape (T60A20, also referred to as M8020) (Weingartner et al., 2003; Arnott et al., 2005; Drinovec et al., 2015)~~for different background scenarios.~~. As aforementioned, the comparison between PP_UniMI and MAAP was reported in Valentini et al. (2020b) where data from BCN and MSY stations were also used to evaluate the performances of PP_UniMI vs MAAP. One of the main objectives of this study was using

175   the multi-wavelength absorption coefficient measurements from the off-line polar photometer extrapolated to the seven AE33 measurement wavelengths to study the wavelength dependence of the AE33 C factor at the three measurement sites.

2 Methodology

2.1 Measurement sites

Aerosols measurements were performed at Barcelona (BCN, urban background, $41°23'24.01''$ N, $02°6'58.06''$ E, 80 m a.s.l.),

180   Montseny (MSY, regional background, $41°46'46''$ N, $02°21'29''$ E, 720 m a.s.l.) and Montsec (MSA, mountain-top, $42°03'05''$ N, $00°43'46''$ E, 1570 m a.s.l.) monitoring supersites (NE Spain). As shown later, these ~~measurement~~ stations are characterized by aerosols with different physical and chemical properties that ~~differently influenced the obtained~~ influenced the differences obtained in the C values. A detailed characterization of the three measurement stations can be found in previous works (e.g. ~~Querol et al. (2001); Rodrıguez et al. (2001); Reche et al. (2011); Brines et al. (2014, 2015); Ealo et al. (2018)~~ Querol et al. (2001); Rodrı

185   BCN; ~~Pérez et al. (2008); Pey et al. (2009); Pandolfi et al. (2011, 2014a, 2016)~~ Pérez et al. (2008); Pey et al. (2009); Pandolfi et al. (2011) MSY; ~~Pandolfi et al. (2014b); Ripoll et al. (2014); Ealo et al. (2016, 2018)~~ Pandolfi et al. (2014b); Ripoll et al. (2014); Ealo et al. (2016) fe MSA). Briefly, BCN station is located within the Barcelona metropolitan area of nearly 4.5 million inhabitants at a distance of about 5 km from the coast. MSY station is located in a hilly and densely forested area, 50 km to the N–NE of the Barcelona and

25 km from the Mediterranean coast. MSA station is located in a remote high-altitude emplacement in the southern side of the
190   Pre-Pyrenees at the Montsec d'Ares Mountain Range, at 140 km to the NW of Barcelona and 140 km to the WNW of MSY.
These supersites are part of the Catalonian Air Quality Monitoring Network, and are part of ACTRIS and GAW networks.
Aerosol optical properties at the three sites were measured following standard protocols (WMO/GAW, 2016).

The area of study is characterized by high concentrations of both primary and secondary aerosols, especially in summer
(Rodríguez et al., 2002; Dayan et al., 2017; Rivas et al., 2020; Brean et al., 2020) from diverse emission sources. Anthropogenic
195   emissions from road traffic, industry, agriculture, and maritime shipping, among others, strongly contribute to the air quality
impairment in this region (Querol et al., 2009b; Amato et al., 2009; Pandolfi et al., 2014c). Moreover, the Mediterranean Basin
is also highly influenced by natural sources, such as mineral dust from African deserts and smoke from forest fires (Bergametti
et al., 1989; Querol et al., 1998; Rodríguez et al., 2001; Lyamani et al., 2006; Mona et al., 2006; Koçak et al., 2007; Kalivitis
et al., 2007; Querol et al., 2009b; Schauer et al., 2016; Ealo et al., 2016; Querol et al., 2019, among others).

200   ## 2.2   Aerosol characterization

2.2.1   Aerosol absorption and eBC measurements

The on-line aerosol absorption coefficient, b_{abs}, was measured at the three sites with a multi angle absorption photometer
(MAAP, Model 5012, Thermo, Inc., USA, Petzold and Schönlinner, 2004)(MAAP, Model 5012, Thermo Inc., USA, Petzold and Schönli
This instrument derives the absorption coefficient at 637 nm (Müller et al., 2011a) and eBC concentration using a radiative
205   transfer model from the measurements of transmission of light through the filter tape and backscattering of light at two different
angles. eBC Black carbon, eBC, and attenuation measurements, b_{atn}, were also performed with the AE33 multi-wavelengths
aethalometer (model AE33, Magee Scientific, Aerosol d.o.o. Drinovec et al., 2015). The AE33 is based on the measurement
at 7 different wavelengths (370, 470, 520, 590, 660, 880, and 950 nm) of the transmission of light through two sample spots
with different flows and particle loading relative to the reference spot. It derives the eBC concentration and the attenuation
210   coefficients by applying eqs. (1) and (2), respectively, following Drinovec et al. (2015):

$$eBC = \frac{S \cdot (\Delta\mathrm{ATN}_1/100)}{F_1(1-\zeta) \cdot \sigma_{abs} \cdot C(1-k\Delta\mathrm{ATN}_1) \cdot \Delta t}; \tag{1}$$

$$b_{atn} = \frac{S \cdot (\Delta\mathrm{ATN}_1/100)}{F_1(1-\zeta) \cdot (1-k\Delta\mathrm{ATN}_1) \cdot \Delta t}, \tag{2}$$

where S is the filter surface area loaded with the sample, F_1 the volumetric flow of the spot 1, ζ the lateral airflow leakage,
σ_{abs} the mass-absorption cross-section, k the loading factor parameter and $\Delta\mathrm{ATN}_1$ the variation of attenuation of light of the
215   filter tape loaded with the sample of the spot 1, ATN_1, during the measurement timestamp Δt.

The Aethalometer absorption coefficient can be derived by dividing the attenuation coefficient (eq. 2) by the multiple scat-
tering parameter C of the filter tape :-

$$b_{abs} = \frac{b_{atn}}{C}. \tag{3}$$

Off-line multi-wavelength particle absorption coefficients were obtained using the PP_UniMI polar photometer (Vecchi et al., 2014; Bernardoni et al., 2017) measurements on the MAAP filter spots. 85 filter spots collected at BCN in the period October 2018 - June 2019, ~~123~~ 126 filter spots collected at MSY between June - December 2018 (Valentini et al., 2020b), and ~~121~~ 122 filter spots collected at MSA between June and November 2018 were analyzed. The time elapsed between the MAAP measurements and the MAAP spots analysis with the PP_UniMI in Milan varied between one year and one month. Once selected and cut, each MAAP spot was stored in a petri dish in a fridge and then sent to Milan. We assumed that there were no major particle losses affecting the measured optical properties, although some volatile compounds could have been evaporated over the period. The PP_UniMI measures the transmitted and scattered radiation at 4 wavelengths (405, 532, 635 and 780 nm) in a range of scattering angles from $0°$ to $173°$ with a resolution down to $0.4°$ and applies a radiative transfer model to derive the absorption coefficients. The PP_UniMI working principle and the detailed analysis of the inter-comparison between the MAAP and PP_UniMI for different measurement sites, including BCN and MSY, was reported in ~~Vecchi et al. (2014); Bernardoni et al. (2017)~~ Vecchi et al. (2014)Bernardoni et al. (2017) and in Valentini et al. (2020b). As mentioned before, in these studies no differences were observed between MAAP and PP_UniMI when the latter was used as a MAAP (PaM), i.e. using a data inversion with similar assumptions as those performed in the MAAP.

Here we ~~first obtained~~ obtain the wavelength dependent attenuation coefficients b_{atn}^λ $b_{atn}(\lambda)$ derived exclusively from the AE33 measurements by multiplying the eBC concentrations provided by the AE33 (eq. 4) by the default wavelength independent instrumental filter ~~value C_{instr}~~ constant C_0 from the AE33 setup file (1.57 for the TFE-coated glass fiber tape T60A20, also referred to as M8020; and 1.39 for the M8060 filter tape),

$$b_{atn}^\lambda(\lambda) = eBC^\lambda(\lambda) \cdot \sigma_{abs}^\lambda(\lambda) \cdot C_{instr \cdot 0} = \frac{S}{F} \frac{\Delta \mathrm{ATN}(\lambda)}{\Delta t} \cdot f(ATN, \lambda) \tag{4}$$

where $f(ATN, \lambda)$ is the function which contains all the corrections, i.e. filter loading and leakage, which are performed by the AE33 for each wavelength (Drinovec et al., 2015). Note that the new filter tape M8060 structurally differs from the old filter tape M8020 in filter fibers material, thickness and density, thus leading to different C_0 values (details can be found in the following online document from Magee Scientific: https://mageesci.com/tape/Magee_Scientific_Filter_Aethalometer_AE_Tape_Replacement_discussion.pdf).

Then, we determined the average and seasonal multiple scattering factor C both as the ratio between the AE33 attenuation coefficients and the absorption coefficients b_{abs}^λ $b_{abs}(\lambda)$ measured by the MAAP and the PP_UniMI (eq. 5), and also by applying a Deming regression between the AE33 attenuation coefficients and the MAAP absorption coefficients for the overall average values for each filter tape.

$$C^\lambda(\lambda) = \frac{b_{atn}^\lambda \, b_{atn}(\lambda)}{b_{abs}^\lambda \, b_{abs}(\lambda)} \tag{5}$$

This value of the multiple scattering parameter ~~C^λ~~ $C(\lambda)$ is the value derived from the experimental comparison of different instruments, contrasting the default instrumental constant value ~~C_{instr}~~ C_0. The data availability at BCN station ranged between

250 2016 and 2020, at MSY and MSA data was measured from 2013 to 2020. Different AE33 filter tapes were used during these periods at the three stations as shown in Fig. S1.

2.2.2 Aerosol scattering measurements

On-line particle total scattering (b_{sp}) and hemispheric backscatter (b_{bsp}) coefficients were measured on-line at the three sites with LED-based integrating nephelometers (Aurora 3000, ECOTECH Pty ,Ltd, Knoxfield, Australia) operating at three wave-

255 lengths (450, 525 and 635 nm). Calibration of the nephelometers was performed three times per year using CO_2 as span gas while zero adjusts were performed once per day using internally filtered particle-free air. The RH threshold was set by using a processor-controlled automatic heater inside the Aurora 3000 nephelometer to ensure a sampling RH of less than 40 % (GAW, 2016). σ_{sp} coefficients were corrected for non-ideal illumination of the light source and for truncation of the sensing volumes following the procedure described in Müller et al. (2011b).

260 ## 2.3 Data treatment and conceptual model

The different analyses performed herein were performed considering the absorption coefficients provided either by the MAAP or the PP_UniMI as reference absorption measurements depending on either time resolution and coverage, or on the measurement availability at several wavelengths. The AE33 and MAAP data (provided with high temporal resolution) were used to study the seasonal variations and the cross-sensitivity to scattering of the C factor. The AE33 and PP_UniMI data (provided

265 with low temporal resolution but at different wavelengths) were used to determine the wavelength dependence of the C factor.

2.3.1 Average, seasonal values analysis and cross-sensitivity to scattering analysis

As aforementioned, the seasonal analysis of the C factor, its average values and the study of its cross-sensitivity to scattering were performed using the long high-time resolution dataset from the MAAP and AE33 measurements at the three measurement sites. For this, we applied eq. (5) using the absorption coefficient from the MAAP and the AE33 attenuation coefficient

270 extrapolated to the 637 nm wavelength of the MAAP through the Ångström exponent obtained from the AE33 measurements at 7 wavelengths.

The cross-sensitivity to scattering which, as shown later, can strongly affect the C factor values, is neglected in AE33 applications where it is generally assumed that the measured light attenuation is only due to the absorption of light by the collected particles (eqs. 1-2). Moreover, it is also generally assumed that the multiple scattering by particles is sample independent,

275 or constant, and can be taken into account by introducing the multiple scattering correction factor C (Drinovec et al., 2015). However, this assumption is a first approximation, since the attenuation of transmitted light is also due to the scattering of light by the collected particles (Bond et al., 1999; Arnott et al., 2005). Taking this dependence into account and following Arnott et al. (2005) ,Schmid et al. (2006) and Segura et al. (2014), we parameterized the light attenuation coefficient as ÷

$$b_{atn} = \frac{S}{F} \frac{\Delta \text{ATN}}{\Delta t} \cdot f(ATN) + m_s \cdot b_{sp}, \tag{6}$$

280   to obtain the relationship between the absorption, attenuation and scattering coefficients ~~:~~

$$b_{abs} = \frac{b_{atn}}{C_f} - m \cdot b_{sp\_}, \tag{7}$$

~~where $f(ATN)$ is the function which contains all the dependencies of the measurement shown in eq. (4), i.e. filter loading correction and leakage, and can be assumed to be close 1 (Schmid et al., 2006).~~

The cross-sensitivity to scattering, which is denoted by the constant m_s, is related with m through $m = m_s/C_f$. Here C_f refers
285   to the filter multiple scattering parameter, that is a value (possibly wavelength dependent) ~~depending~~ that depends only on filter properties. If we rearrange eq. (7) by expressing the scattering coefficient through the single scattering albedo, we obtain the dependence of the absorption as a function of SSA (eq.8)~~. Following eq. 5, we obtain the multiple scattering parameter, C_f, but the effective C actually measured, C_{eff}, is~~, similarly to eq. 17 in Schmid et al. (2006). The measured multiple parameter, C, affected by the cross-sensitivity to ~~the scattering coefficient,~~ scattering can be expressed as shown in eq. (9).

290    $$b_{abs} = \frac{b_{atn}}{C_f} \cdot \frac{1}{1 + m \cdot \frac{SSA}{1-SSA}} \tag{8}$$

$$C_{eff} = C_f \left(1 + m \cdot \frac{SSA}{1-SSA}\right) = C_f + m_s \cdot \frac{SSA}{1-SSA} \tag{9}$$

The effective multiple scattering parameter~~C_{eff} is derived from the comparison of the~~, C, depends on the physical properties of collected particles. By comparing data from different instruments (AE33, MAAP, and nephelometer) ~~and therefore includes the properties of collected particles, and, consequently, also any sensitivity of the measurement to the sample properties~~
295   ~~other than absorption. The most important cross-sensitivity is due to scattering . The~~ we were able to parameterize the cross-sensitivity of the C to scattering (eq. 8). Eq.9 shows that the actual AE33 cross-sensitivity to scattering is more pronounced when the measured aerosol particles have higher SSA~~(eq. 9)~~, whereas for particles with lower SSA ~~it becomes closer~~ eq.9 converges to eq. ~~(5)~~5.

By analyzing the dependency of the effective multiple scattering parameter C with the SSA we ~~can obtain the experimental~~
300   ~~constants of the filter properties~~ obtained the experimental fit constants (C_f and m_s) that describe the relationship between C and SSA. Furthermore, ~~given that~~ we will present in Section 3.1 how the cross-sensitivity to scattering of C ~~depends on the physical and optical (both extensive and intensive) properties of collected particles, we can study its dependency on the shape, size and mixing state of the collected aerosol particles (see Section 3.1 and Supplementary material~~depended on some intensive aerosol particle optical properties that strongly depend on aerosol particles size distribution and chemical composition (Figs.
305   S3-S5).

The AE33 data treatment applied to obtain the C seasonality and the cross-sensitivity to scattering included a pre-process filtering method following the approach suggested in Springston and Sedlacek (2007) and Backman et al. (2017). This filtering method consists on setting a threshold value for the measured attenuation variation, ΔATN_1, high enough so that the signal-to-noise ratio is large; herein we have used a fixed value of 0.01. As can be deduced from eq. (1), the faster the fixed ΔATN_1
310   is reached, the shorter is the period Δt, implying therefore a higher eBC concentration value during the same period. The

method we employed determines the period at which the ΔATN_1 step was reached, and recalculated the eBC concentration for this Δt. As a consequence of this eBC re-calculation, we filtered out the noise resulting from very small values close to the detection limit of the instrument while maintaining the higher eBC values measured without introducing a bias to the measurements as is the case when averaging. With the aim to study the seasonality of the C factor and its cross-sensitivity to scattering, we averaged $b_{abs,MAAP}$ and b_{sp} coefficients to match the corresponding AE33 variable timestamp, Δt, which ranged approximately between 3 and 14 min (cf. Fig. S2). Moreover, the time granularity of the measurements varied between 1 to 5 minutes, depending on the software used for data logging (see Table S1). Given the length of the measurement periods, we assumed that the AE33 filter tapes considered here were characterized under a wide range of aerosol particle properties typically observed at the measurement stations and that the non-simultaneity of AE33 measurements with the two filter tapes did not prevent the comparison between the obtained C.

2.3.2 Wavelength dependence analysis

To study the wavelength dependence of the C factor we compared the absorption coefficients at several wavelengths measured with the PP_UniMI with the attenuation coefficients obtained from the AE33 (eq. 5). Since the off-line PP_UniMI measurements were performed on the MAAP spots, the ~~AE33 attenuation coefficients~~ measured attenuation and scattering coefficients from AE33 and nephelometer, respectively, were averaged over the timestamp of each one of the selected MAAP spots. The absorption coefficients from the PP_UniMI were inter/extrapolated to the seven AE33 wavelengths using the ~~absorption~~ attenuation Ångström exponent, obtained through a log-log fit from the PP_UniMI absorption measurements.

Valentini et al. (2020b) reported that the MAAP overestimates the absorption coefficient compared to the PP_UniMI. For BCN and MSY Valentini et al. (2020b) reported a MAAP overestimation of 18% and 21%, respectively. By applying the same methodology as in Valentini et al. (2020b) we obtained a difference between MAAP and PP_UniMI for MSA of 19% (Fig. A1) similar to the biases obtained for BCN and MSY. For this reason, Valentini et al. (2020b) also studied the comparison between MAAP and PP_UniMI using for the PP_UniMI data inversion the same assumptions as those performed in the MAAP (PaM approach) and reported a 1:1 correlation between the two instruments. Given that most of the aethalometer C values reported in literature were obtained by comparing AE33 attenuation measurements and MAAP absorption measurements, we report here also the median C values obtained comparing the AE33 with the PP_UniMI (Table S2) and with PaM (Table S3).

3 Results

3.1 Multiple scattering ~~correction factor: Average values and seasonal variation~~ parameter cross-sensitivity to scattering

~~Here we present the seasonal cycle~~ The cross-sensitivity to scattering of the C factor ~~calculated at~~ at the three stations was obtained by analyzing the relationship between the multiple scattering parameter C (at 637 nm) and the measured SSA (eq. 9).

Table 1. AE33 multiple scattering parameter C for some measurement stations (included BCN, MSY and MSA) and cross-sensitivity to scattering for BCN, MSY and MSA station compared to literature values for AE33 TFE-coated glass (M8020). Different approaches, as aforementioned in Section 3.2, have been used to obtain the factor C. Since the literature values are obtained through either one of the methods, we include these vales in its corresponding column (C or C_{Deming}).

Site	Characteristics	Filter type	Reference	C	C_{Deming}	C_f	m_s (%)
Barcelona	Urban background	M8020	This study	**2.29 ± 0.49**	**1.99± 0.02**	-	-
		M8060	This study	**2.44 ± 0.57**	**2.20 ± 0.02**	**2.50 ± 0.02**	**1.6 ± 0.3**
Leipzig	Urban background	M8020	Müller (2015)	3.2			
		M8020	Bernardoni et al. (2020)		2.78		
Rome	Urban background	M8060	Valentini et al. (2020a)	2.66			
Klagenfurt	Urban background	M8020	Drinovec et al. (2020)	1.57			
Montseny	Regional background	M8020	This study	**2.29 ± 0.46**	**2.05 ± 0.02**	**2.21 ± 0.01**	**1.8 ± 0.1**
		M8060	This study	**2.23 ± 0.30**	**2.13 ± 0.01**	**1.96 ± 0.01**	**3.0 ± 0.1**
Montsec d'Ares	Mountain-top	M8020	This study	**2.36 ± 0.59**	**2.21 ± 0.03**	**1.96 ± 0.02**	**3.4 ± 0.1**
		M8060	This study	**2.51 ± 0.71**	**2.05 ± 0.02**	**1.82 ± 0.02**	**4.9 ± 0.1**
Mt. Bachelor	Mountain-top	M8020	Laing et al. (2020)	4.24			

The SSA was obtained independently at 637 nm ~~at~~ using simultaneous MAAP and multiple-wavelength integrating nephelometer data. C was obtained through eq. (5) from the AE33 attenuation coefficient, extrapolated at 637 nm using the AAE from AE33, and the MAAP absorption coefficients at 637 nm. The analysis was performed by binning the SSA data using Freedman and Diaconis (1981) and then averaging the obtained C values within each SSA bin. Binned data were then fitted following (9) to obtain the experimental values of both C_f and m_s.

Figure 1 and Table 1 show the results of the fit for BCN, MSY and MSA ~~. For this, we used the AE33 attenuation measurements extrapolated to the MAAP wavelength of 637 nm and divided the attenuation by the absorption measurements provided by the MAAP (eq. 5).~~ for both M8020 and M8060 filter tapes. Moreover, Table 1 compares the C values obtained here with those reported in literature for the M8020 filter tape. For M8020, we calculated a constant C_f of 2.21 ± 0.01 and a cross-sensitivity to scattering, m_s, of 1.8 ± 0.1 at MSY, and of 1.96 ± 0.02 and 3.4 ± 0.1 % at MSA. For the M8060 filter tape, the fit yielded a multiple scattering constant C_f of 2.50 ± 0.02 and a cross-sensitivity to scattering of 1.6 ± 0.3 % at BCN, a C_f of 1.96 ± 0.01 and a m_s of 3.0 ± 0.1 % at MSY, and a constant C_f of 1.82 ± 0.02 and a m_s of 4.9 ± 0.1 % at MSA.

As a consequence of the cross-sensitivity to scattering, we can appreciate in Fig. 1 a clear increase of C with increasing SSA with an up to 3-fold increase of C for SSA>0.90-0.95 depending on the station and filter tape considered. The cross-sensitivity to scattering was evident for both filter tapes at the regional (MSY) and mountain (MSA) stations where the probability of measuring SSA higher than 0.90-0.95 was high (57-70% of the data in Fig. 1). Conversely, at the urban site (BCN), where the SSA was on average lower (12% of SSA data was above 0.90), a lower cross-sensitivity to scattering was observed. This significant increase of the C factor at high SSA, if not accounted for, can lead to a large overestimation of both eBC

concentrations and absorption coefficients from Aethalometer instruments. This effect can have a larger impact at sites where high SSA values are typically observed as remote arctic sites and mountain-top sites (Collaud Coen et al., 2004; Gyawali et al., 2009; Andre as well as in places where increasing or decreasing trends of SSA have been observed (Collaud Coen et al., 2020). This cross-sensitivity to scattering of the filter explains the higher C factors obtained on average at these types of sites (Table 1) and suggests the need of using either a site-specific C, or a C that takes into account the SSA measured by an independent absorption method. Given its impact on the absorption coefficient, this effect needs to be taken into account for climate studies.

In order to further characterize the observed cross-sensitivity to scattering, we explored how the variations of C with SSA depended on different aerosol particle intensive optical properties, namely AAE (Fig. S3), backscatter fraction (BF; Fig. S4) and single scattering albedo Ångström exponent (SSAAE; Fig. S5). We found that large C values, and high SSA, were often obtained when the sampled aerosol composition was dominated by mineral dust during Saharan dust outbreaks, as demonstrated by the occurrence of negative SSAAE at high SSA (Fig. S5). In fact, Saharan dust outbreaks, which are common in the WMB (Escudero et al., 2005; Querol et al., 2004, 2009b, a; Ealo et al., 2016; Querol et al., 2019; Yus-Díez et al., 2020), have the potential to increase the SSA above the average velues especially at the regional (MSY) and remote (MSA) stations (e.g. Pandolfi et al., 2014a). In prior studies, negative values of the SSAAE have been associated with an aerosol mixture dominated by mineral dust (Collaud Coen et al., 2004; Ealo et al., 2016; Yus-Díez et al., 2020). Moreover, we observed that high C values (for SSA>0.95) were also associated with AAE values higher than around 1.5 (cf. Fig. S3) thus indicating a relatively higher absorption efficiency of the collected particles in the UV, consistent with the presence of either dust or brown carbon (BrC) particles (Kirchstetter et al., 2004b; Chen and Bond, 2010; Zotter et al., 2017; Forello et al., 2019, 2020). Furthermore, low BF values, indicative of the predominance of large particles, were also on average associated with high SSA values (cf. Fig. S4). Note that the dependence of the C vs. SSA on the aforementioned intensive optical properties was not clearly observed in BCN, where, at least for the period under study, local pollution masked the effects of coarse dust particles on the measured intensive optical properties and on SSA which kept values lower than around 0.90-0.95. The observed dependency of C on aerosol particle intensive optical properties demonstrated that both particle size distribution and chemical composition can affect the reported C vs. SSA relationships.

3.2 Multiple scattering correction factor: Average values and seasonal variation

Here we present the average values and the seasonal cycle of the C factor calculated at 637 nm at BCN, MSY and MSA. We analyzed the multiple scattering parameter C values ~~through both~~ both through a Deming regression, taking into account the measurement error of the MAAP ~~(Petzold and Schönlinner, 2004, 12%;)~~ (12%; Petzold and Schönlinner, 2004) and of the AE33 (15%; Zanatta et al., 2016; Rigler et al., 2020), and by calculating the median value of the C factor ~~as the ratio of the AE33 attenuation coefficient and the MAAP absorption measurements (cf. eq. 5). In the latter case, the~~ density distribution. The uncertainties of the C factor were derived as ~~the~~ either the methodological error from the regression slope of the Deming fit, or as the half-width at half maximum (HWHM) of the density distribution of the C factor~~whereas, in the case of the Deming regression, we used the methodological error from the regression slope.~~. We present here the results from both the aforementioned methods
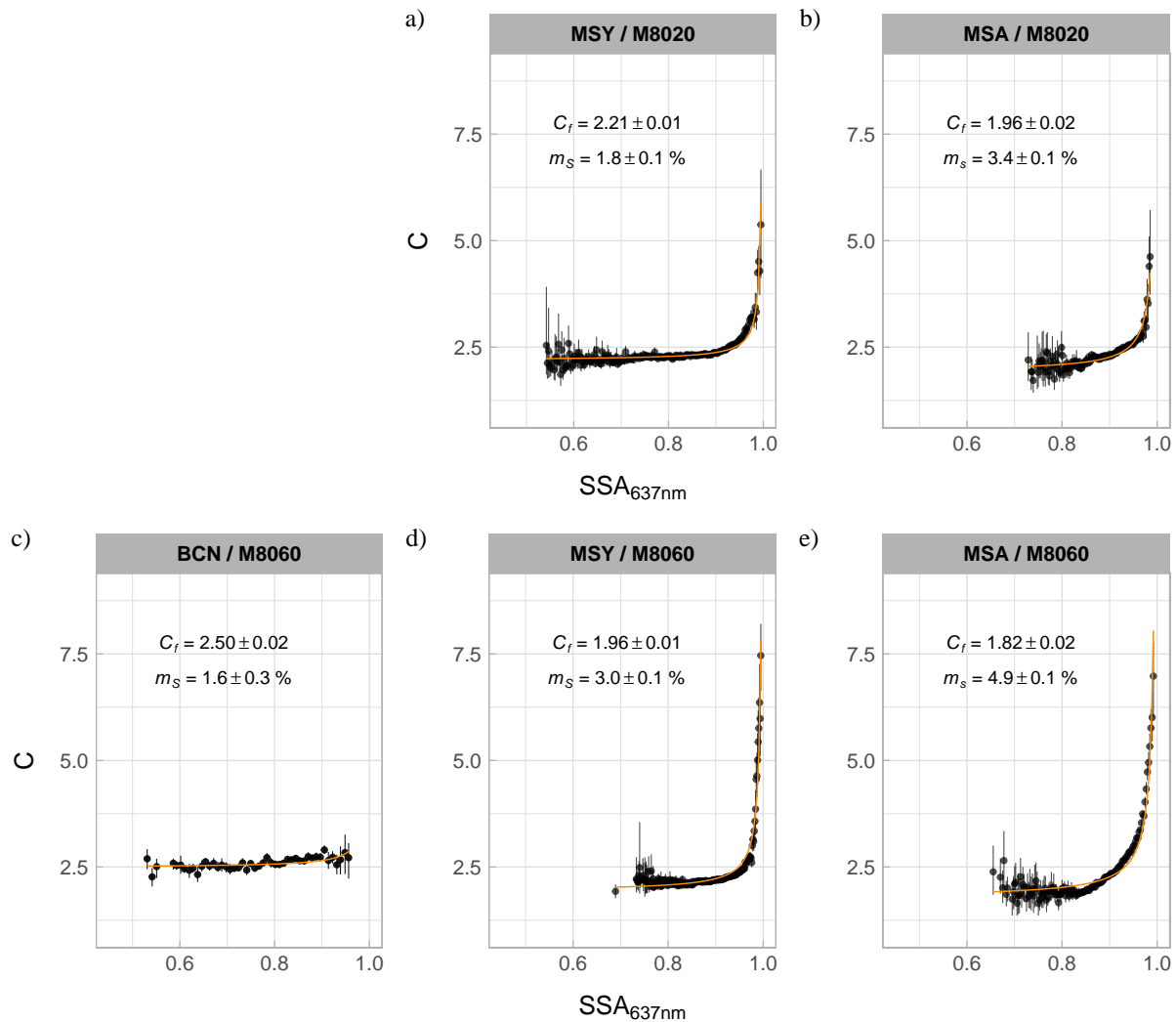
Figure 1. Cross-sensitivity to scattering analysis for TFE-coated glass tape (also known as M8020, upper panel) and M8060 filter tape (lower panel) for BCN (c), MSY (a,d) and MSA (b,e) stations obtained by attenuation coefficients from the AE33, absorption coefficients from the MAAP photometer and scattering coefficients from the integrating nephelometer. Each data point represents the mean, and the vertical bars the first and third quartile for each bin. Multiple scattering constant, C_f and cross-sensitivity to scattering, m_s, are determined by fitting eq. (9) to the binned data.

because both methods have been reported in literature (e.g. Backman et al., 2017; Bernardoni et al., 2020, ; c.f. Table 1 in this work).

395

The density distribution of the C factor obtained from the ratio (with a variable time resolution, as aforementioned in Sect. 2.3.1), showed a quasi-Gaussian distribution at the three measurement sites with a small tail toward higher C values (Fig. 2).

The median values of the C factor for the M8020 filter tape were 2.29 ± 0.48, 2.29 ± 0.46, 2.36 ± 0.59 for BCN, MSY and MSA, respectively. These values were on average similar or slightly lower (with differences less than a 7%) compared to the median C values obtained for the M8060 filter tape of 2.44 ± 0.57, 2.23 ± 0.30, and 2.51 ± 0.71 (cf. Table 1). The Deming regression fit results (Fig. S6) showed C values of 1.99 ± 0.02, 2.05 ± 0.02, and 2.21 ± 0.03 (at BCN, MSY and MSA, respectively) for the M8020 which were slightly lower (with differences <10%) compared to the C values of 2.20 ± 0.02, 2.13 ± 0.01, and 2.05 ± 0.02 obtained for the M8060. Note that the uncertainties from the Deming regression were lower compared to the uncertainties derived as HWHM of the distributions because the Deming regressions were performed using binned data (cf. Fig. S6). This also was the likely explanation for the lower C values on average obtained with the Deming regression compared to the median values of the density distribution. The difference of the C values between both methods ranged between 4-18% depending on the filter tape/measurement station considered (cf. Table 1). However, both methods were consistent and provided higher C factor for the M8060 than for the M8020 filter tape.

As reported in Table 1, overall, higher C values were found at MSA, where both the SSA and the cross-sensitivity of the filter tape to scattering were higher compared to MSY and BCN (cf. Figs. 1 and S7). The C values for the AE33 M8020 and M8060 filter tapes obtained at urban background stations in Rome (Valentini et al., 2020a) and Leipzig (Müller, 2015; Bernardoni et al., 2020) were in the same range as those found in this work for BCN (Table 1).

Figure 3 shows the seasonal variability of the C factor for the TFE-coated glass and M8060 filter tapes at the three stations. It can be appreciated the large variability of the C parameters (cf. Fig. 3) at the three sites during all the seasons, consistent with the width of the C factor density distribution (Fig. 2) and the SSA seasonal evolution variability (Fig. S7).

On average, an increase of C was observed at MSY and MSA in summer (JJA) for both filter tapes. This increase was likely driven by a greater influence of diurnal processes and the impact of the atmospheric boundary layer (ABL) during the warm months at these two elevated stations, and by changes in the chemical and physical
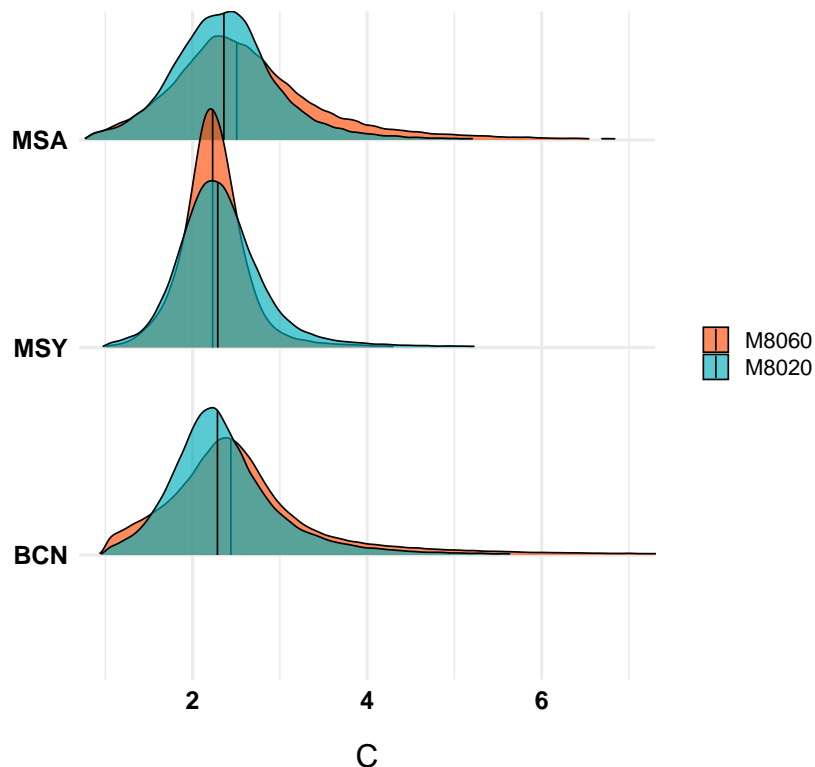
Figure 2. Density distribution of the C factor for each filter type, M8020 and M8060, as obtained through eq. (5) using both attenuation coefficient from the AE33 and the absorption coefficient from the MAAP. The vertical line represents the median value of each distribution.

properties of collected particles in summer compared to winter (DJF). In fact, spring and summer seasons in the WMB are characterized by a high frequency of Saharan dust outbreaks ~~(e.g. Pey et al., 2013)~~ (e.g. Pey et al., 2013; Yus-Díez et al., 2020) and

435 formation of high concentrations of secondary organic aerosols and secondary sulfate particles (e.g. Ripoll et al., 2015) which in turn increase the particle scattering efficiency and the SSA in summer compared to winter (Pandolfi et al., 2011). ~~As shown later, high SSA increases the C values above the commonly measured values . In BCN, however, the C~~ Although dust particles can absorb radiation (e.g. Sokolik and Toon, 1999; Di Biagio et al., 2019), the effect of Saharan dust outbreaks at the measurement stations considered here was to increase the SSA (at 637 nm) over the average values. In fact, as shown

440 by Pandolfi et al. (2014b), both scattering and absorption increased at MSY and MSA during Saharan dust outbreaks, but the resulting SSA was higher compared to other atmospheric scenarios typical of the area under study. Therefore, the higher C values observed during Saharan dust outbreaks were coherent with an increase of SSA over the threshold above which the C sharply increased (cf. Fig. 1, S3, S4 and S5). An increase of the C when dust particles are deposited on the filter tape was also reported by Di Biagio et al. (2017) for the AE31 aethalometer. Di Biagio et al. (2017) reported C values for dust particles by
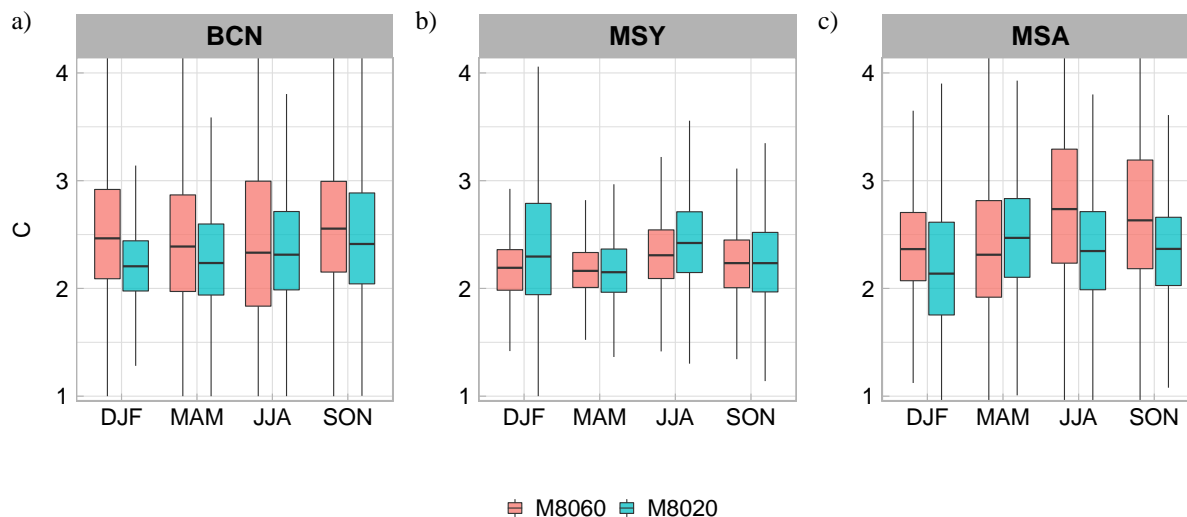
Figure 3. Seasonal evolution of the C factor at a) BCN, b) MSY and c) MSA measurement stations for both TFE-coated glass (M8020) and M8060 filter tapes. The box plot boxes show the range between the first and third quartile (IQR) with the median value for each season distribution represented by the inner line; the maximum whisker length is proportional to 1.5 times the third and first quartile difference, or inter-quartile range (1.5 · IQR).

445   generating particles by mechanical shaking of dust samples from different desert soils using AE31 and MAAP measurements, and reported C values between 3.6 and 3.96 for Saharan desert soils (Table 2 of Di Biagio et al. (2017)).

As shown in Sect. 3.1, high SSA increased the C values, and, consequently, the C seasonality was affected, to some degree, by the SSA seasonality. In fact, Fig. S7 in the supplementary material shows that the seasonal evolution of the SSA at MSY and MSA mirrored quite well the seasonal evolution of the C, with an increase of both C and SSA toward the warm season.

450   In BCN, the inter-season variability of both C and SSA was less pronounced and the C remained fairly constant during the different seasons ~~likely because of its greater influence to season-independent local pollutant sources~~. Exception was in the winter period (DJF) when both C (M8060) and SSA showed minima. Nevertheless, the variability within each season was the largest in BCN, due to a higher variability of the SSA values at this station within each season compared to MSY and MSA ~~.~~ (Fig. S7). The relationship between C and SSA can be also observed in Fig. S8, where the diel cycles of both C and

455   SSA were reported. In BCN, both C and SSA showed two relative minima in the morning and in the afternoon, mirroring the traffic rush hours. At MSY, the sea-breeze-driven transport of pollutants in the afternoon caused a reduction of both SSA and C. Conversely, at MSA both C and SSA showed less variability in the diel cycles and less similarity was observed. Note that the similarities commented above between the diel/seasonal cycles of C and SSA were more or less evident depending on the season/station considered. In fact, we have shown in Fig. 1 that high SSA (> 0.90-0.95) can strongly affect the C values, but

460   less dependency between C and SSA was observed for lower SSA thus also contributing to mask the similarities between C and SSA reported in Figs. 3, S7, and S8 which were obtained averaging all available data, including C values at lower SSA.

3.3 Wavelength dependence analysis from the PP_UniMI vs AE33 comparison

~~The~~

The spectral dependence of the AE33 C ~~$_{eff}(\lambda)$ factorand its spectral dependence (Fig. 4)~~factor, $C(\lambda)$, was studied at the three stations by comparing the attenuation coefficients, b_{atn}, from AE33 at seven different wavelengths with the absorption coefficients, b_{abs}, from the PP_UniMI. To this aim, the PP_UniMI absorption coefficients were inter/extrapolated to the seven AE33 wavelengths using the Absorption Ångström Exponent (AAE) obtained from the original PP_UniMI measurements. The obtained mean AAE were 1.12 ± 0.17, 1.29 ± 0.24, and 1.35 ± 0.18 for BCN, MSY, and MSA stations, respectively, with an increase from the urban (BCN) to the regional (MSY) and remote (MSA) ~~site~~ sites due to the increase in the relative importance of non-fossil BC sources (~~i.e.~~e.g. biomass burning) and Saharan dust at the remote sites compared to BCN.

~~Wavelength dependence of C at BCN, MSY and MSA comparing b_{atn} from the AE33 measured at each wavelength and b_{abs} inter/extrapolated to the same wavelength from the PP_UniMI. Box plots have been obtained as in Fig. 3 with the addition of the mean value of the distribution for each wavelength represented by a marker. The values above the box plots between adjacent wavelengths and between 370 and 950 nm wavelength box plots show the obtained p-values, with p<0.05 meaning a statistically significance difference.~~

~~At~~ Fig. 4 shows that at the urban (BCN) and ~~the~~ regional (MSY) stations the C factor did not ~~show any~~ present a statistically significant dependence with the wavelength~~(Fig. 4). However,~~. However, Fig. 4c shows that at the remote MSA station the multiple scattering parameter C ~~showed (Fig. 4)~~ presented a statistically significant increase between 370 (~~C_{eff}~~nm (C=3.47) and 950 nm (~~C_{eff}~~C=4.03) ~~wavelengths~~ (cf. Table S2). The observed increase of the C factor with ~~the wavelength can affect~~ wavelength affects the absorption coefficients derived from the AE33 attenuation measurements and, consequently, can affect all the intensive optical parameters such as ~~the absorption Ångström exponent (AAE) or the single scattering albedo (SSA)~~ AAE, SSA and SSAAE which can be derived from the ~~multi-wavelengths~~ multi-wavelength AE33 absorption measurements and scattering coefficient measurements. Moreover, a wavelength-dependent C factor can ~~have an impact on~~ impair aethalometer based BC source apportionment analysis, such as the Aethalometer model, used to determine the contribution from fossil fuels vs biomass burning emissions (Sandradewi et al., 2008). ~~Weingartner et al. (2003) and Segura et al. (2014) found no wavelength dependence for the multiple scattering parameter~~ Contradictory results have been reported in literature about the spectral dependence of C for older versions of aethalometer (model AE31)~~, whereas Bernardoni et al. (2020) found~~. For example, Weingartner et al. (2003) found strong indication of the independence of C with wavelength, and neither Segura et al. (2014) found any wavelength dependence of the multiple scattering parameter C with the wavelength. Conversely, Bernardoni et al. (2020) observed a decrease of the C factor with wavelengths, although it was not statistically significant~~, and reported the impact of the wavelength dependent C on source apportionment model results.~~.

~~Virkkula et al. (2015) and Drinovec et al. (2017) have shown that the AE33 factor loading parameter, k, increases with increasing BF (smaller particles) and decreases with increasing SSA and that the wavelength dependence of k also depends on these two optical properties. Moreover, Drinovec et al. (2017) have shown that~~ As can be appreciated by comparing Figs. 2, 3 and Fig. 4, the multiple scattering correction factors obtained using the PP_UniMI reference instrument were larger than
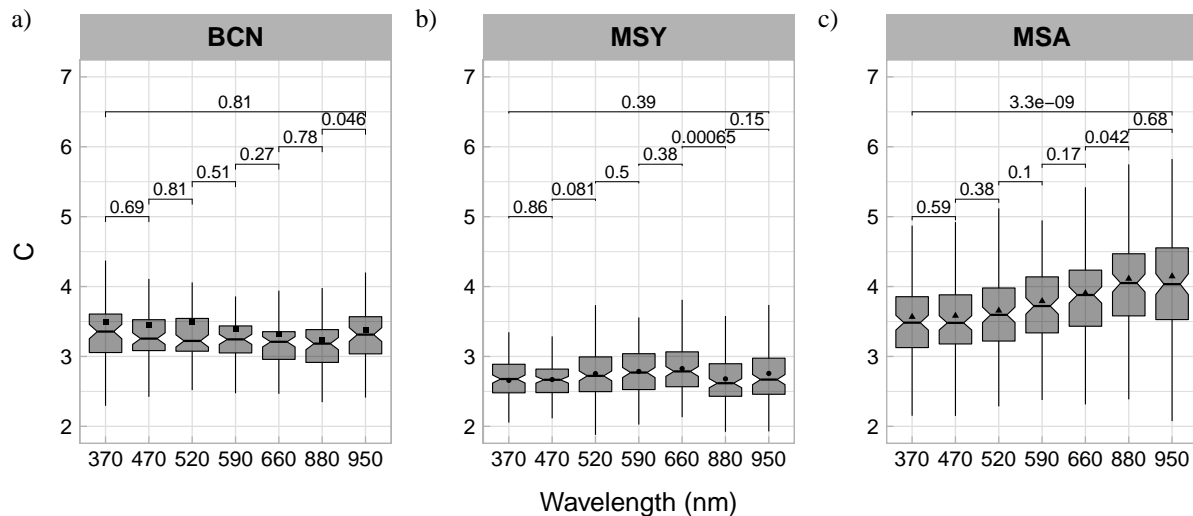
Figure 4. Wavelength dependence of C at BCN, MSY and MSA comparing b_{atn} from the AE33 measured at each wavelength and b_{abs} inter/extrapolated to the same wavelength from the PP_UniMI. Box plots have been obtained as in Fig. 3 with the addition of the mean value of the distribution for each wavelength represented by a marker. The values above the box plots between adjacent wavelengths and between 370 and 950 nm wavelength box plots show the obtained p-values, with p<0.05 meaning a statistically significance difference.

those obtained with the ~~BC coating reduces the k at longer wavelengths for higher SSA . Thus, particle size, ageing and BC-coating processes can potentially affect the AE33 factor loading k.~~ MAAP as a consequence of the offset in the absorption measurements between MAAP and PP_UniMI. A detailed discussion of this offset can be found in Fig. A1 and in Fig. 2 in Valentini et al. (2020b).

500 ~~In order to understand the likely reasons causing the observed dependence of the C with wavelength at MSA, we performed a similar analysis as in Virkkula et al. (2015) by comparing the C and its wavelength dependence with different aerosol particles intensive optical properties. Figure ?? shows the wavelength-dependence of the factor C (i.e. the slope of C vs. wavelength, a_C) with SSA , BF,~~ Hereafter, we propose a possible explanation for the different spectral dependencies found for the C at the measurement sites considered here. We have shown in Section 3.1 that, independently from the measurement station

505 considered, the cross-sensitivity to scattering can strongly increase the C for SSA values above an upper threshold. To explore if the SSA can also affect the C wavelength dependence, we studied the wavelength dependence of the C for SSA values above and below the site-dependent SSA thresholds. Figure 5 shows the comparison between the C factor at MSY and MSA for SSA above (high SSA), and below (low SSA) the SSA thresholds of 0.95 and ~~the single-scattering albedo Ångström exponent (SSAAE)at the three sites.~~ 0.9, respectively, for MSY and MSA (cf. Fig. 1). Fig. 5 shows that at MSA there was a statistically

510 significant increase of C with the wavelength for SSA>0.90, whereas no statistically significant increase was observed for SSA<0.90. For this specific analysis, based on the PP_UniMI off-line measurements, 86% of SSA values at MSA (68 samples out of 79) were above the SSA threshold of 0.95. At MSY, only 1 sample out of 126 was characterized by SSA value higher

Figure 5. Wavelength dependence of C at MSY (a,c) and MSA (b,d) obtained comparing b_{atn} from the AE33 measured at each wavelength and b_{abs} inter/extrapolated to the same wavelength from the PP_UniMI. Box plots have been obtained as in Fig. 3 and separated into two categories depending whether the SSA was above (high ssa, upper panel) or below (low ssa, lower panel) the threshold at which C sharply increases. As in Fig. 3, the values above the box plots between adjacent wavelengths and between 370 and 950 nm wavelength box plots show the obtained p-values, with p<0.05 meaning a statistically significance difference.

than the SSA threshold of 0.95, thus preventing a robust statistical analysis of the C wavelength dependence for high SSA at MSY. Despite this, a 17% increase of C with the wavelength, from 2.85 at 370 nm to 3.43 at 950 nm, for this single point was observed (cf. Fig. 5a). At MSY, similarly to MSA, the C did not show any dependence with the wavelength for SSA<0.95 (cf. Fig.5c). Thus, this analysis demonstrated that high SSA of the particles deposited on the filter tape can increase the C values, influencing at the same time its wavelength dependence.

Figure **??** shows no clear relationship of a_C with SSA and BF at BCN and MSY. At MSA, however, Figures **??**c,f show that a_C increased with an increasing SSA and decreased with an increasing BF; i. e. variations of BF and SSA can cause the factor C to change as a function of the wavelengths. In Sect. 3.1 we will show (Fig. S9) that high SSA was related to the presence of dust from Saharan deserts (Saharan dust outbreaks). Thus, the increase of C slope with decreasing BF (larger particles) and with increasing SSA at MSA was likely caused by Saharan dust outbreaks affecting the station. To further demonstrate the role of dust particles in a_C, Fig. **??**i shows that the a_C at MSA was the highest when the SSAAE was negative. In fact, negative SSAAE values have been related to the predominance of dust particles in the atmosphere (e.g. Collaud Coen et al., 2010; Ealo et al., 2016). Indeed, Ealo et al. (2016) have shown that the ability of a SSAAE to indicate the presence of dust in the atmosphere strongly depends on the relative importance of fine particles from local sources, and that the SSAAE can detect a higher number of Saharan dust outbreaks at MSA, due to its remote location, compared to MSY where local meteorology (i. e. sea breeze) effectively transports every day fine particles from the urbanized/industrialized coastline where BCN is located. Nevertheless, as shown We have shown in Section 3.1 that the sharp increase of C at high SSA at the stations herein analyzed can be associated with the presence of particles dominated by dust, characterized by low SSAAE and BF and high AAE and SSA (Figs. S3, S4 and S5). Therefore, we performed a similar C spectral dependence analysis as in Fig. 6b, the comparison between the C factor calculated during 5, but separating the days affected by Saharan dust and during days not affected by dust revealed that the slope at MSA remained positive also for (dust) and the days without dust influence (no-dust days, suggesting that other particle properties contributed to the positive aC observed at mountain-top station. In addition, Figures 6a, b show that when the MSY and MSA stations were affected by Saharan dust, the factor C increased at all wavelengths compared to non-dust days with a major effect observed at MSA compared to MSY. We will present later in this paper that high SSA determined an increase of the C and that, at the stations considered here, high SSA was always associated to presence of dust from Saharan deserts 3.1.

Figure 6. Wavelength dependence of C at MSY (a,c) and MSA (b,d) obtained comparing b_{atn} from the AE33 measured at each wavelength and b_{abs} inter/extrapolated to the same wavelength from the PP_UniMI. Box plots have been obtained as in Fig. 3 and separated into two categories depending whether Saharan dust outbreaks took place (dust) or not (no-dust). As in Fig. 3, the values above the box plots between adjacent wavelengths and between 370 and 950 nm wavelength box plots show the obtained p-values, with p<0.05 meaning a statistically significance difference.

540 ~~Wavelength dependence of C at a) MSY and, b) MSA comparing b_{atn} from the AE33 measured at each wavelength and b_{abs} inter/extrapolated to the same wavelength from the PP_UniMI. Box plots have been obtained as in Fig. 3 and separated into two categories depending whether Saharan dust outbreaks took place (dust) or not (no-dust).~~

~~For the study period considered here, the lack of wavelength-dependence of C at BCN and MSY could be~~). As shown in Fig. 6, no spectral dependence of C was observed during either dust and no-dust scenarios at MSY. This lack of dependence with the dust intrusions could be due to the limited number of off-line samples at MSY characterized by high SSA (1 out of 126). Thus,

545 due to the ~~increased relative importance of local anthropogenic particles at these stations compared to MSA~~ low temporal resolution of off-line PP_UniMI measurements, even during Saharan dust ~~outbreaks (Pandolfi et al., 2014b). Furthermore, Figs. **??**g,h show that (based on the data available in this work) the SSAAE was positive at BCN and slightly negative at MSY keeping positive values for the majority of the analyzed samples. Thus, we hypothesize that at MSA the increase in the relevance~~ days the SSA at MSY rarely increased above the SSA threshold. Nevertheless, using high-time resolution data (cf.

550 Fig. 1) the potential effect of dust particles ~~during Saharan dust outbreaks had a larger effect (compared to MSY and BCN) on the wavelength dependence of the Cfactor. However. as already noted (Fig. **??**i) , the slope of the C factor at MSA was the highest when SSAAE was strongly negative but kept positive values also when SSAAE was higher than zero suggesting that dust particles may not be the only reason for the observed increase of C with the wavelength at MSA.~~

~~For completeness, we present in~~ to increase the SSA (and consequently the C) was evident at both MSY and MSA. At

555 MSA (cf. Fig. 6) the ~~following the dependence of the k factor and its slope with~~ C showed a statistical significant increase with wavelength for both dust and no-dust samples due to the fact the the samples with high SSA at MSA (86%) were well distributed between the two scenarios. Thus, these results confirmed that the ~~wavelength (a_k) with BF and SSA as done by Virkkula et al. (2015). Since~~ SSA was the main parameter that influenced the spectral behaviour of the C parameter.

To further explore the possible causes that contributed to the different C spectral dependencies observed, we performed a

560 similar analysis as in Virkkula et al. (2015) by comparing the C and its wavelength dependence with different aerosol particles intensive optical properties, namely: SSA, BF and SSAAE. Virkkula et al. (2015) and Drinovec et al. (2017) have shown that the AE33 factor loading parameter, k, increases with increasing BF (smaller particles) and decreases with increasing SSA and that the wavelength dependence of k ~~is intrinsic to the AE33 instrument, for the sake of the analysis we have used the largest dataset at our disposal (Fig. S1), following the data processing mentioned in Sect.2.3.1. As shown in Fig. S4, a_k was negative~~

565 also depends on these two optical properties as well as on the particle mixing state. In Fig. S9 we present a similar analysis by studying the effects of these intensive optical properties on the multiple scattering parameter C instead of k. Fig. S9 shows the slope of C with the wavelength (i.e. the ~~k decreased with increasing wavelength) for SSAvalues higher than 0.5, 0.75 and 0.85~~

~~at BCN, MSY and MSA, respectively. The relationship between k and SSA (inset graphs in Fig. S4)was similar to that between~~ ~~a $_k$ and SSA~~ wavelength-dependence of C) with SSA, BF, and SSAAE at the three sites. No clear relationship was observed between the C slope and the three intensive optical properties at both BCN and MSY. Moreover, the C slope at these two sites were close to zero for the considered intensive optical properties. The observed lack of C gradient was again likely due to the fact that at BCN and MSY the SSA did not exceed the threshold value, even when the SSAAE indicated the possible presence of Saharan dust intrusions at MSY (cf. Fig. S9h). However, Fig. S9c shows that at MSA there was a shift of the C slope toward large positive values when SSA was above 0.95. Below this SSA threshold value, the C slope was close to zero confirming the reduced C wavelength dependence for low SSA values at MSA. Moreover, when the SSAAE(BF) at MSA (cf. ~~A decrease of a$_k$ with increasing SSA has been also reported by Virkkula et al. (2015) for an urban environment in China (Nanjing)~~. Fig. ~~S4 implies that for darker aerosols, the factor loading correction increases with wavelength,~~ S9i and ~~that, at higher SSA, k decreases with wavelength. Furthermore, at BCN the a$_k$ increased with BF and kept negative values (i. e.~~ S9f) decreased towards negative(low) values (Saharan dust intrusions), the slope of the C increased, again confirming the potential of coarse Saharan dust to increase the SSA and, consequently, the C especially at the remote site. Note that, as already commented (cf. Fig. 6), the ~~correction decreased with increasing wavelength) up to a BF of 0.2; thereafter, for very fine particles (i. e. BF~~ C slope kept positive values at MSA also for the samples not dominated by dust (SSAAE>~~0.2) the slope of k became positive, indicating that the correction increased with wavelength. Virkkula et al. (2015) also reported an increase of a$_k$ with increasing BF in Nanjing urban environment; however the a$_k$ was positive starting from BF values higher than 0.14. At MSY and MSA the a$_k$ was always negative (i. e. the correction decreased with increasing wavelength) even if the relationship between a$_k$ (and k) and BF at MSY and MSA was not linear as observed for BCN.~~ 0), thus further indicating the predominance effect of SSA on the C wavelength dependence. Thus, the results presented in Fig. S9 confirmed the effects of SSA on the C presented in Fig. 5 and 6.

~~Figure 7 shows the results of the~~ The lack of points for BCN (none) and MSY (1 of 126) for large SSA values, specially above the SSA threshold obtained in Fig. 1, prevented from extrapolating the results to other measurement background conditions and further studies should be performed to better characterize the spectral behaviour of C and its dependency with the cross-sensitivity to scattering under different atmospheric conditions/scenarios. This is specially important, as already commented, in view of the contradictory results reported in literature (e.g. Weingartner et al., 2003; Segura et al., 2014; Bernardoni et al., 2 The results presented here clearly indicated that when the SSA exceeded a given site-dependent threshold, as determined using the method in Sect. 3.1, the C values and its wavelength dependence increased. For the measurement sites considered here, Saharan dust outbreaks were identified as possible cause for SSA values higher than the threshold. However, from a general point of view, other factors, including the location of the measurement stations and/or absence of anthropogenic pollution, can determine the presence of a particle mixture with high or very high SSA.

Finally, we performed a sensitivity study on the effects that ~~the~~ using a wavelength-dependent C (C(λ)) had on the ~~calculated AAE compared to the~~ AAE derived from AE33 measurements, comparing the results with those obtained using the usual approach based on the application of a constant C factor (C$_{\overline{const}}$ ~~)for all AE33 wavelengths. For BCN and MSY measurement stations,~~ (const)). Figure 7 shows that the AAE values ~~did not show~~ for BCN and MSY did not present any significant vari-

Figure 7. The absorption Ångström exponent (AAE) calculated with a constant C(const) and the wavelength-dependent $C(\lambda)$ for all stations. Box plots have been obtained as in Figs. 3 and 4, with the markers indicating the mean AAE values.

ation (cf. Table S4)~~with~~, with AAE mean values of 1.19 ± 0.15 and 1.27 ± 0.12 (at BCN and MSY, respectively) ~~using a constant C~~ ~~and slightly decreasing to~~ for C(const), and 1.17 ± 0.15 and 1.25 ± 0.12 (for BCN and MSY, respectively) ~~when~~

605 ~~the wavelength-dependent C was used. At MSA,~~ for $C(\lambda)$. These results for BCN and MSY were coherent with the observed lack of spectral dependence of C at these two stations (Fig. 4). However, at MSA the observed increase of the C with the wavelength ~~caused the AAE to increase by~~, introduced an increase of the AAE of around 13%, from 1.19 ± 0.07 (~~constant C~~C(const)) to 1.35 ± 0.07 (~~wavelength-dependent C). Similarly to the above sensitivity study on the calculated AAE~~C(λ)). Similarly, Fig. ~~S5 reports the SSA calculated using the~~ S10a,b present the results of a sensitivity analysis performed to

610 understand the effects that using a constant or a wavelength-dependent C ~~factor in comparison with the SSA obtained using the~~ ~~constant C factor~~ had on the SSA at 470, 660 and 950 nm. As ~~reported in Fig. S5,~~ for the AAE, Fig. S10c shows no significant variation of SSA at the 3 considered wavelengths at BCN and MSY, again consistent with the observed lack of dependence of the C factor with wavelength at these two sites. However, Fig. S10 shows a statistically significant increase of the SSA at MSA station of around 1.3% ~~for~~ at 660 nm ~~,~~ and 2% ~~for~~ at 950 nm ~~was observed when using the wavelength-dependent C~~ ~~compared~~

615 ~~to a constant C. This increase~~ when using $C(\lambda)$ instead of C(const). Conversely, as expected, no statistically significant change was appreciated at the lower wavelength, 470 nm. This variation introduced by $C(\lambda)$ on AAE and SSA, although not large, is relevant since it occurs at the threshold of SSA value for which a substantial increase of the C as a function of SSA was observed, as shown in Section 3.1. ~~As for the AAE, Fig.S5 shows no significant variation for the SSA values at the 3 wavelengths~~ ~~at BCN and MSY~~ ~~consistent with the observed lack of dependence of the C factor with wavelength.~~

620 **3.4** ~~Multiple scattering parameter cross-sensitivity to scattering~~

~~The~~

4 Conclusions

In this work we studied the multiple scattering parameter C for two filter tapes used in AE33 dual-spot aethalometers, i.e. the previously used M8020 and the currently used M8060 filter tapes. For this, we used data collected at three different background

625 stations in NE Spain: an urban background station in Barcelona, BCN, a regional background station at Montseny, MSY, and a mountain-top station at Montsec d'Ares, MSA. We obtained the C correction factor comparing the AE33 attenuation measurements with the absorption coefficients measured from MAAP instruments, and used simultaneous scattering measurements from an integrating nephelometer to characterize the cross-sensitivity to scattering of ~~the C factor~~ C. Moreover, we studied the C wavelength dependence at the three ~~stations was obtained by analyzing the relationship between the multiple scattering~~

630 ~~parameter C_{eff} (at 637 nm) and SSA.~~

~~SSA was obtained independently at 637 nm using simultaneous MAAP and nephelometer data. C_{eff} was obtained through~~ ~~eq. (5) using the~~ sites comparing the AE33 attenuation ~~coefficient extrapolated at 637 nm using the AAE from AE33 and the~~ ~~MAAP absorption coefficients at 637 nm. The analysis was performed with SSA measurements binned using Freedman and Diaconis (1981)~~ ~~and with the average C_{eff} obtained for each bin. The fit of the binned multiple scattering parameter (eq. 5) following eq. (9)~~

635 ~~yields the experimental values of both C_f and m_s.~~ coefficients with the absorption coefficients from the off-line multi-wavelength PP_UniMI .

~~Figure 1c and Table 1 show the results of the fit for BCN,~~ We presented here a novel approach to characterize the cross-sensitivity to scattering of the C correction factor. This approach consisted in fitting the measurements of the C versus SSA. The fits provided the constant C_f and a cross-sensitivity factor m_S. We applied the fits to the M8020 filter tape at MSY and MSA, and

640 we obtained higher cross-sensitivity values of the C factor (1.8±0.1% and 3.4±0.1% at MSY and MSA ~~for both filter tapes: the~~ ~~TFE-coated glass filter tape (M8020) and the currently distributed~~ , respectively) compared to those reported in the literature (around 1-1.5 %). For the first time, we characterized here the cross-sensitivity to scattering also of the new M8060 filter tape. ~~For the TFE-coated glass~~ We obtained a higher cross-sensitivity to scattering for the M8060 than for the M8020 filter tape, ~~it~~ ~~was found a constant of 2.21 ± 0.01 and a cross-sensitivity to scattering of 1.8 ± 0.1 at MSY, and of 1.96 ± 0.02 and 3.4 ±~~

645 ~~0.1 % for C_f and m_s, respectively,~~ with values of 1.6±0.3%, 3.0±0.1% and 4.9±0.1% for BCN, MSY and MSA, respectively. The multiple scattering parameter, C_f, for the M8020 filter tape was 2.21 ± 0.01 at MSY and 1.96 ± 0.02 at MSA. For the M8060 filter tape ~~, the fit yields a multiple scattering constant C_f of 2.50 ± 0.02 and a cross-sensitivity to scattering of $1.6 \pm$~~ ~~0.3 %~~ the fit led to C_f values of 2.50 ± 0.02 at BCN, ~~a C_f of 1.96 ± 0.01 and a m_s of 3.0 ± 0.1 %~~ 1.96 ± 0.01 at MSY, and ~~a~~ ~~constant C_f of 1.82 ± 0.02 and a m_s 4.9 ± 0.1 %~~ 1.82 ± 0.02 at MSA.

650 ~~AE33 multiple scattering parameter C for some measurement stations (included BCN, MSY and MSA) and cross-sensitivity~~ ~~to scattering for BCN, MSY and MSA station compared to literature values for AE33 TFE-coated glass (M8020, TFE in~~ ~~the table). Different approaches, as explained in Section 3.2, have been used to obtain the factor C.Site Characteristics~~

Filter type Reference C C$_{Deming}$ C$_f$ m$_s$ (%) **Barcelona** Urban background TFE This study **2.29 ± 0.49 1.99± 0.02 – –** M8060 This study **2.44 ± 0.57 2.20 ± 0.02 2.50 ± 0.02 1.6 ± 0.3** Leipzig Urban background TFE Müller (2015) 3.2 TFE Bernardoni et al. (2020) 2.78 Rome Urban background M8060 Valentini et al. (2020a) 2.66 Klagenfurt Urban background TFE Drinovec et al. (2020) 1.57 **Montseny** Regional background TFE This study **2.29 ± 0.46 2.05 ± 0.02 2.21 ± 0.01 1.8 ± 0.1** M8060 This study **2.23 ± 0.30 2.13 ± 0.01 1.96 ± 0.01 3.0 ± 0.1 Montsec d'Ares** Mountain-top TFE This study **2.36 ± 0.59 2.21 ± 0.03 1.96 ± 0.02 3.4 ± 0.1** M8060 This study **2.51 ± 0.71 2.05 ± 0.02 1.82 ± 0.02 4.9 ± 0.1** Mt. Bachelor Mountain-top TFE Laing et al. (2020) 4.24

As a consequence of the The consequence of this cross-sensitivity to scattering we can appreciate in Fig. 1a , 1b, 1d, and 1e an resulted in a large increase of the C values, up to 3-fold increase of C for SSA >0.95, for SSA values above 0.9-0.95. This significant increase of the C factor at high SSA, if not accounted for, can lead to a large overestimation of both the eBC concentrations and the absorption coefficients absorption coefficients measured by aethalometers. This can be especially relevant at sites typically characterized by an aerosol mixture with high SSA. This effect can have a larger impact at sites where very high SSA values are typically observed as remote arctic sites, mountain-top sites, or sites where aerosol is dominated by mineral dust, among others (Collaud Coen et al., 2004; Pandolfi et al., 2014b, 2018), as well as in places where there are trends of increasing or decreasing SSA(Collaud Coen et al., 2020). This In fact, the effect of this cross-sensitivity to scattering of C was the likely reason explaining the filter explains the higher C factors obtained on average at these types of sites (Table 1) and suggests the need of using either a site-specific C, or a C that takes into account the SSA measured by an independent absorption method. This effect needs to be taken into account for climate studies.

We interpreted the differences in the obtained C$_f$ values reported in literature for mountain-top and Arctic measurement stations. Here, we observed larger C values and m$_s$ values as variations dependent on other sample properties. Size distribution and the mixing state are the most obvious. We studied the dependence of the higher cross-sensitivity to scattering obtained at BCN, MSY and MSA on different optical parameters (Fig. S6, S7, S8 and S9). We found that the large C values at high SSA were mostly obtained when the sampled aerosol composition was dominated by mineral dust (such as during Saharan dust outbreaks) as demonstrated by the negative Ångström exponent of the SSA (SSAAE) at high SSA. Thus, in prior studies, negative values of the SSAAE have been associated with an aerosol mixture dominated by mineral dust (Collaud Coen et al., 2004; Ealo et al., 2016; Yus-Díez et al., 2020). Moreover, we have found AAE values higher than 1.5 above a SSA of 0.95 (Fig. S6), thus implying a relatively higher absorption fraction in the UV range whether by dust absorbing particles or by BrC aerosols (Kirchstetter et al., 2004b; Chen and Bond, 2010; Zotter et al., 2017; Forello et al., 2019, 2020). Furthermore, we have found, as already mentioned in Sect. 3.3, different behaviour of the C and the factor loading,k, at MSA versus BCN and MSY; Fig. S7, S8, S9 show an increase of the C factor with increasing SSA , decreasing BF, and a SSAAE<0, which can be related to the larger relevance of absorbing dust particles. Fig. S7 and S8 shows that at BCN, while the BF remains constant with an increasing SSA, k decreases, yet the C factor does not show a great increase. This description for our set of sites is coherent with the different aerosol sources, especially the common Saharan dust outbreaks affecting the WMB (Escudero et al., 2005; Querol et al., 2004, 2009b, a; Ealo et al., 2016; Querol et al., 2019; Yus-Díez et al., 2020). at the

mountain station and much less C variability at the urban site, where the SSA rarely exceeded the SSA threshold from which changes in C can be observed.

Cross-sensitivity to scattering analysis for TFE-coated glass tape (also known as M8020, upper panel) and M8060 filter tape (lower panel) for BCN (c), MSY (a,d) and MSA (b,e) stations obtained by attenuation coefficients from the AE33, absorption coefficients from the MAAP photometer and scattering coefficients from the integrating nephelometer. Each data point represents the mean, and the vertical bars the first and third quartile for each bin. Multiple scattering constant, C_f and cross-sensitivity to scattering, m_s, are determined by fitting eq. (9) to the binned data.

The multiple scattering parameter C for the AE33 dual-spot aethalometer using different tapes materials, the previously used TFE-coated glass and the Overall, the main difference between the two filter tapes studied here was the higher cross-sensitivity to scattering observed for the currently used M8060 filter tapes, has been analyzed using data collected at three different background stations in NE Spain: an urban background station in Barcelona, BCN, a regional background station at Montseny, MSY, and a mountain-top station at Montsec d'Ares, MSA. We obtained the C correction factor comparing the AE33 attenuation coefficient measurements with the absorption coefficients measured by a MAAP and used simultaneous scattering measurements from an integrating nephelometer for analyzing the cross-sensitivity to scattering. Moreover, we analyzed the C wavelength dependence at the three sites comparing the AE33 attenuation coefficient measurements with the multi-wavelength PP_UniMI absorption coefficientstape compared to the previously used M8020 filter tape. Despite the different cross sensitivity to scattering, both filter tapes showed average C values which fall within the measurement uncertainties.

We have found an average multiple scattering parameter C at 637 nm of 2.29, 2.29, 2.36 for the TFE-coated glass filter tape (M8020) M8020 filter tape and of 2.44, 2.23 and 2.51 for the M8060 filter tape, for BCN, MSY and MSA measurement stations, respectively. The obtained C factor showed a seasonal variability at Due to the dominant effect of SSA on the C, the obtained C factors showed seasonal and diel variability at the three sites that mirrored the variability of SSA. At MSY and MSA with a maximum at higher C values were on average observed in summer due to the changes in the physical-chemical aerosol properties that led to SSA values on average higher in summer than in winter. A larger fraction of dust particles and formation of secondary organic aerosols and secondary sulfates likely explained the observed increase of C in summer at these regional/remote sites. However, at the urban background station of BCN the C values remain fairly constant throughout the year.

We also analyzed the wavelength dependence of C the C parameter for the M8060 filter tape for at BCN, MSY and MSA . We by comparing the AE33 attenuation data with the off-line PP_UniMI absorption measurements performed on selected MAAP spots. Overall, we found a statistically significant increase with the wavelength, from 3.47 for 370 nm to 4.03 for 950 nm for at the mountain-top station of MSA(MSA), whereas at BCN an and MSY background stations no statistically significant dependence was found. The reason for the lack of wavelength dependence of the C at BCN and MSY was the lack of MAAP spots characterized by high SSA. Thus, due to the low temporal resolution of off-line PP_UniMI measurements, the SSA at MSY and, especially, at BCN rarely increased above the SSA threshold. Conversely, the wavelength-dependence of C at the mountain station was in part due to the predominance of dust particles during high probability of measuring SSA values higher than the site-dependent SSA threshold, from which the C values start to increase. For this analysis, we studied the C

wavelength dependence separately for samples characterized by high SSA (higher than the site-dependent threshold) and low SSA and observed that at MSA no dependence of the C with the wavelength was observed for samples with low SSA, whereas a clear dependence was observed for the sample with high SSA. Thus, the analysis presented here demonstrated that high SSA of the particles deposited on the filter tape can increase the C values influencing at the same time its wavelength dependence. Interestingly, only one sample (out of 126) collected at MSY regional station was characterized by high SSA and for this sample the calculated C strongly increased with wavelength. The results presented here clearly indicated that when the SSA exceeded a given site-dependent threshold, the C values and its wavelength dependence increased. For the measurement sites considered here, Saharan dust outbreaks ~~at this station.~~ were identified as possible cause for SSA values higher than the threshold. However, other factors,including the location of the measurement stations and/or the absence of anthropogenic pollution, can determine the presence of a particle mixture with high or very high SSA. We also investigated the effect of considering a wavelength-dependent C at MSA station compared ~~with~~ to using a constant C on the absorption Ångström exponent (AAE) and the single scattering albedo (SSA) through sensitivity tests. Results revealed an increase of the AAE by 13% and an increase of the SSA by 1.3% when using the wavelength-dependent C factor compared to using a constant C factor (i.e. with no λ–dependence). This effect may impact any source apportionment method which takes into account the multi-wavelength absorption values from the AE33 (e.g. the Aethalometer model). ~~Furthermore, although no statistically significant difference with wavelength was found for the C factor for BCN and MSY, using a wavelength-dependent C instead of a constant one has the potential of modifying the results from the derived intensive optical properties and source apportionment models~~

In summary, based on the results herein presented, the absorption coefficients from AE33 data can be corrected with different degrees of confidence depending on the information available to estimate the multiple scattering parameter C:

- A tailored dynamic multiple scattering parameter can be obtained if on-line simultaneous reference absorption measurements are available. In this case, a dynamic C with high temporal resolution can be obtained, allowing an in-situ correction of AE33 data and allowing studying, for example, diel/seasonal cycles of the multiple scattering parameter. Here we used on-line MAAP absorption measurements at one wavelength for the determination of a dynamic C at the same MAAP wavelength.

  ~~We presented a novel approach for analyzing the cross-sensitivity to scattering of the C correction factor. This approach consisted in fitting the measurements of the C versus SSA. The fits provided the constant C_f and a cross-sensitivity factor m_S. We have applied the fits to the TFE-coated glass filter tape at MSY and MSA and we obtained similar results for the cross-sensitivity factor (1.8±0.1% and 3.4±0.1%, respectively) compared to those reported in the literature (around 1-1.5 %). For the first time here we characterized the cross-sensitivity to scattering also of the new M8060 filter tape. We obtained a cross-sensitivity to scattering for the M8060 of 1.6±0.3%, 3.0±0.1% and 4.9±0.1% for BCN, MSY and MSA, respectively. The~~

- If independent reference multi-wavelengths absorption measurements are available, then the dependence of the multiple scattering parameter with wavelengths can be studied. Here we determined the wavelength dependence of the multiple scattering parameter C by using the polar photometer (PP_UniMI) off-line absorption measurements performed on the

MAAP filter spots and by comparing the off-line PP_UniMI measurements with AE33 attenuation data integrated over the MAAP filter spots time stamp.

- – If reference absorption measurements are not available for the experimental determination of the C, then the average values of the multiple scattering parameter ~~, C_f for each station and filter tape obtained from the fit for the TFE-coated~~
760 ~~glass filter tape is $C_f = 2.21 \pm 0.01$ at MSY, and $C_f = 1.96 \pm 0.02$ at MSA. The M8060 filter tape values are : $C_f = 2.50 \pm 0.02$ at BCN, $C_f = 1.96 \pm 0.01$ at MSY, and $C_f = 1.82 \pm 0.02$ at MSA. The consequence of this cross-sensitivity to scattering is the large increase of the C values, up to 3-fold, for SSA values above 0.9-0.95. As a result of this large increase, actual absorption coefficients and eBC concentrations are much lower than those reported by~~ provided here for three different measurement stations can be used as reference.

765 - – If both independent reference absorption measurements and scattering measurements are available, then the cross sensitivity to scattering of the ~~AE33 when the aerosol particles measured have a high SSA (e.g. aged particles, desert dust particle outbreaks, etc.). The effect of this cross-sensitivity to scattering pattern of C is responsible for the higher C values measured at mountain-top and Arctic measurement stations~~multiple scattering parameter C can be determined by studying the relationship between C and single scattering albedo (SSA). In this case, a parameterization can be obtained relating
770 C and SSA.

  ~~The methodology of this study for the C correction factor analysis is of great importance for the retrieval of more accurate aerosol absorption coefficients and equivalent black carbon concentrations at several wavelengths from AE33 instruments. With the approach presented here, the wavelength dependence of the C factor and its cross-sensitivity to scattering can be derived. The C~~

775 - – If SSA measurements are not available, this work provides parameterized formulas that allow calculating C over a wide range of SSA values.

Finally, the C values obtained in this work for different station types (urban, regional, remote) may serve as reference for similar background measurement sites where the ~~same methodology~~ methodology presented here cannot be applied. ~~Yet~~Nevertheless, discrepancies may arise due to the possible differences in aerosol sources, composition and mixing state
780 at different sites ~~and~~that, accordingly, ~~to the different aerosol particles compositions and mixing states~~will results in different aerosol particle optical properties. Similar analysis ~~for~~ performed at other measurement sites with similar features may reduce the uncertainties around the applicability of the results presented here to other stations.

Appendix A: Absorption coefficient relationship between a MAAP and a PP_UniMI polar photometer for MSA station

785 This appendix aims to show the result of applying the same methodology as in Section 3.1 of Valentini et al. (2020b) to the PP_UniMI analyzed dataset for obtaining the bias for the MSA station in the absorption coefficient measurements between the
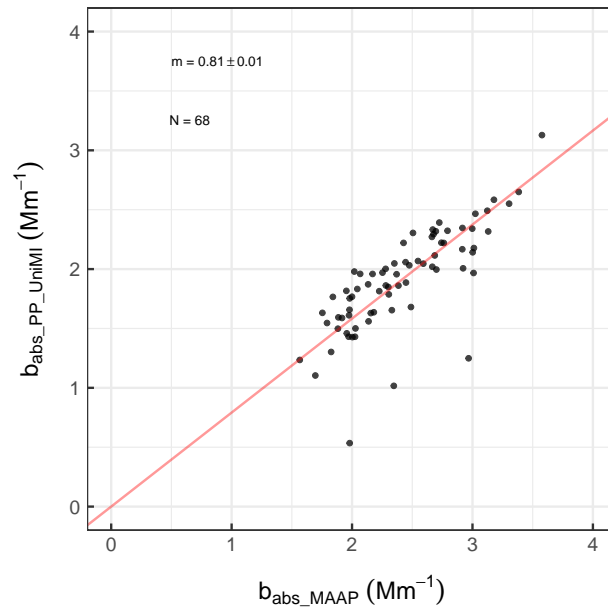
Figure A1. Comparison between the aerosol absorption coefficient measured by PP_UniMI on sample spots ($\sigma_{ap\_PP\_UniMI}$) and the MAAP photometer (σ_{ap_MAAP}).

MAAP and the PP_UniMI polar photometer A1. It consists on the application of a Deming regression fit, which results in a slope of 0.81 ± 0.01 for our dataset.

Code and data availability. The Montseny and Montsec data sets used for this publication are accessible online on the WDCA (World Data Centre for Aerosols) web page: http://ebas.nilu.no. The Barcelona data sets were collected within different national and regional projects and/or agreements and are available upon request. The code used for analysis can be obtained upon request to the corresponding author.

Author contributions. DC, SV, RV and VB performed and analyzed the measurements with the PP_UniMI polar photometer. NP, CR, MP, AA and JYD carried out the maintenance and supervision of the BCN, MSY and MSA supersites. AA, GM, MP and XQ played a crucial role in the processes of shaping the manuscript structure as well as helping with the data analysis. JYD developed the data process, the analysis of the results, and summarized and expressed them in this manuscript. All authors provided advice regarding the manuscript structure and content as well as contributed to the writing of the final manuscript.

Competing interests. At the time of the research, MR and MI were also employed by the manufacturer of the Aethalometer AE33.

Acknowledgements. Measurements at Spanish sites (Barcelona, Montseny and Montsec d'Ares) were supported by the Spanish Ministry of Economy, Industry and Competitiveness and I+D+I "Retos Colaboración" funds under the CAIAC project (PID2019-108990PB-100), by the Generalitat de Catalunya (AGAUR 2017 SGR41 and the DGQA) and the European Commission via ACTRIS-IMP (project 871115). We acknowledge support of the COST Action CA16109 COLOSSAL. GM acknowledges support from the Slovenian Research Agency program P1-0385 "Remote sensing of atmospheric properties". IDAEA-CSIC is a Centre of Excellence Severo Ochoa (Spanish Ministry of Science and Innovation, Project CEX2018-000794-S).

800

References

Ajtai, T., Filep, Á., Schnaiter, M., Linke, C., Vragel, M., Bozóki, Z. Á., Szabó, G., and Leisner, T.: A novel multi-wavelength photoacoustic spectrometer for the measurement of the UV-vis-NIR spectral absorption coefficient of atmospheric aerosols, Journal of Aerosol Science, 41, 1020–1029, https://doi.org/10.1016/j.jaerosci.2010.07.008, 2010.

Alfaro, S., Lafon, S., Rajot, J., Formenti, P., Gaudichet, A., and Maille, M.: Iron oxides and light absorption by pure desert dust: An experimental study, Journal of Geophysical Research: Atmospheres, 109, 2004.

Amato, F., Querol, X., Alastuey, A., Pandolfi, M., Moreno, T., Gracia, J., and Rodriguez, P.: Evaluating urban PM10 pollution benefit induced by street cleaning activities, Atmospheric Environment, 43, 4472–4480, 2009.

Andreae, M. O. and Gelencsér, A.: Black carbon or brown carbon? the nature of light-absorbing carbonaceous aerosols, Atmospheric Chemistry and Physics, 6, 3131–3148, https://doi.org/10.5194/acp-6-3131-2006, 2006.

Andrews, E., Ogren, J., Bonasoni, P., Marinoni, A., Cuevas, E., Rodríguez, S., Sun, J. Y., Jaffe, D., Fischer, E., Baltensperger, U., et al.: Climatology of aerosol radiative properties in the free troposphere, Atmospheric Research, 102, 365–393, 2011.

Arnott, W. P., Hamasha, K., Moosmüller, H., Sheridan, P. J., and Ogren, J. A.: Towards aerosol light-absorption measurements with a 7-wavelength aethalometer: Evaluation with a photoacoustic instrument and 3-wavelength nephelometer, Aerosol Science and Technology, 39, 17–29, https://doi.org/10.1080/027868290901972, 2005.

Backman, J., Schmeisser, L., Virkkula, A., Ogren, J. A., Asmi, E., Starkweather, S., Sharma, S., Eleftheriadis, K., Uttal, T., Jefferson, A., Bergin, M., Makshtas, A., Tunved, P., and Fiebig, M.: On Aethalometer measurement uncertainties and an instrument correction factor for the Arctic, Atmospheric Measurement Techniques, 10, 5039–5062, https://doi.org/10.5194/amt-10-5039-2017, 2017.

Bergametti, G., Dutot, A.-L., Buat-Menard, P., Losno, R., and Remoudaki, E.: Seasonal variability of the elemental composition of atmospheric aerosol particles over the northwestern Mediterranean, Tellus B: Chemical and Physical Meteorology, 41, 353–361, 1989.

Bergstrom, R. W., Pilewskie, P., Russell, P. B., Redemann, J., Bond, T. C., Quinn, P. K., and Sierau, B.: Spectral absorption properties of atmospheric aerosols, Atmospheric Chemistry and Physics, 7, 5937–5943, https://doi.org/10.5194/acp-7-5937-2007, 2007.

Bernardoni, V., Valli, G., and Vecchi, R.: Set-up of a multi wavelength polar photometer for off-line absorption coefficient measurements on 1-h resolved aerosol samples, Journal of Aerosol Science, 107, 84 – 93, https://doi.org/https://doi.org/10.1016/j.jaerosci.2017.02.009, http://www.sciencedirect.com/science/article/pii/S0021850216301549, 2017.

Bernardoni, V., Ferrero, L., Bolzacchini, E., Forello, A. C., Gregori, A., Mo, G., Prati, P., Rigler, M., Santagostini, L., Soldan, F., Valli, G., and Vecchi, R.: Determination of Aethalometer multiple-scattering enhancement parameters and impact on source apportionment during the winter 2017-2018 EMEP / ACTRIS / COLOSSAL campaign in Milan ., 2020.

Bond, T. C., Anderson, T. L., and Campbell, D.: Calibration and Intercomparison of Filter-Based Measurements of Visible Light Absorption by Aerosols, Aerosol Science and Technology, 30, 582–600, https://doi.org/10.1080/027868299304435, 1999.

Bond, T. C., Doherty, S. J., Fahey, D., Forster, P., Berntsen, T., DeAngelo, B., Flanner, M., Ghan, S., Kärcher, B., Koch, D., et al.: Bounding the role of black carbon in the climate system: A scientific assessment, Journal of Geophysical Research: Atmospheres, 118, 5380–5552, 2013.

Brean, J., Beddows, D., Shi, Z., Temime-Roussel, B., Marchand, N., Querol, X., Alastuey, A., Minguillón, M. C., and Harrison, R. M.: Molecular insights into new particle formation in Barcelona, Spain, Atmospheric Chemistry and Physics, 20, 10 029–10 045, 2020.

Brines, M., Dall'Osto, M., Beddows, D. C., Harrison, R. M., and Querol, X.: Simplifying aerosol size distributions modes simultaneously detected at four monitoring sites during SAPUSS, Atmospheric Chemistry and Physics, 14, 2973–2986, https://doi.org/10.5194/acp-14-2973-2014, 2014.

Brines, M., Dall'Osto, M., Beddows, D. C., Harrison, R. M., Gómez-Moreno, F., Núñez, L., Artíñano, B., Costabile, F., Gobbi, G. P., Salimi, F., Morawska, L., Sioutas, C., and Querol, X.: Traffic and nucleation events as main sources of ultrafine particles in high-insolation developed world cities, Atmospheric Chemistry and Physics, 15, 5929–5945, https://doi.org/10.5194/acp-15-5929-2015, 2015.

Cappa, C. D., Zhang, X., Russell, L. M., Collier, S., Lee, A. K., Chen, C. L., Betha, R., Chen, S., Liu, J., Price, D. J., Sanchez, K. J., McMeeking, G. R., Williams, L. R., Onasch, T. B., Worsnop, D. R., Abbatt, J., and Zhang, Q.: Light Absorption by Ambient Black and Brown Carbon and its Dependence on Black Carbon Coating State for Two California, USA, Cities in Winter and Summer, Journal of Geophysical Research: Atmospheres, 124, 1550–1577, https://doi.org/10.1029/2018JD029501, 2019.

Chen, Y. and Bond, T. C.: Light absorption by organic carbon from wood combustion., Atmospheric Chemistry & Physics, 10, 2010.

Collaud Coen, M., Weingartner, E., Schaub, D., Hueglin, C., Corrigan, C., Henning, S., Schwikowski, M., and Baltensperger, U.: Saharan dust events at the Jungfraujoch: detection by wavelength dependence of the single scattering albedo and first climatology analysis, pp. 2465–2480, 2004.

Collaud Coen, M., Weingartner, E., Apituley, A., Ceburnis, D., Fierz-Schmidhauser, R., Flentje, H., Henzing, J. S., Jennings, S. G., Moerman, M., Petzold, A., Schmid, O., and Baltensperger, U.: Minimizing light absorption measurement artifacts of the Aethalometer: Evaluation of five correction algorithms, Atmospheric Measurement Techniques, 3, 457–474, https://doi.org/10.5194/amt-3-457-2010, 2010.

Collaud Coen, M., Andrews, E., Alastuey, A., Arsov, T. P., Backman, J., Brem, B. T., Bukowiecki, N., Couret, C., Eleftheriadis, K., Flentje, H., Fiebig, M., Gysel-Beer, M., Hand, J. L., Hoffer, A., Hooda, R., Hueglin, C., Joubert, W., Keywood, M., Kim, J. E., Kim, S.-W., Labuschagne, C., Lin, N.-H., Lin, Y., Lund Myhre, C., Luoma, K., Lyamani, H., Marinoni, A., Mayol-Bracero, O. L., Mihalopoulos, N., Pandolfi, M., Prats, N., Prenni, A. J., Putaud, J.-P., Ries, L., Reisen, F., Sellegri, K., Sharma, S., Sheridan, P., Sherman, J. P., Sun, J., Titos, G., Torres, E., Tuch, T., Weller, R., Wiedensohler, A., Zieger, P., and Laj, P.: Multidecadal trend analysis of aerosol radiative properties at a global scale, Atmospheric Chemistry and Physics Discussions, 2020, 1–54, https://doi.org/10.5194/acp-2019-1174, https://www.atmos-chem-phys-discuss.net/acp-2019-1174/, 2020.

Collaud Coen, M., Andrews, E., Lastuey, A., Petkov Arsov, T., Backman, J., Brem, B. T., Bukowiecki, N., Couret, C., Eleftheriadis, K., Flentje, H., Fiebig, M., Gysel-Beer, M., Hand, J. L., Hoffer, A., Hooda, R., Hueglin, C., Joubert, W., Keywood, M., Eun Kim, J., Kim, S. W., Labuschagne, C., Lin, N. H., Lin, Y., Lund Myhre, C., Luoma, K., Lyamani, H., Marinoni, A., Mayol-Bracero, O. L., Mihalopoulos, N., Pandolfi, M., Prats, N., Prenni, A. J., Putaud, J. P., Ries, L., Reisen, F., Sellegri, K., Sharma, S., Sheridan, P., Patrick Sherman, J., Sun, J., Titos, G., Torres, E., Tuch, T., Weller, R., Wiedensohler, A., Zieger, P., and Laj, P.: Multidecadal trend analysis of in situ aerosol radiative properties around the world, Atmospheric Chemistry and Physics, 20, 8867–8908, https://doi.org/10.5194/acp-20-8867-2020, 2020.

Corbin, J. C., Pieber, S. M., Czech, H., Zanatta, M., Jakobi, G., Massabò, D., Orasche, J., El Haddad, I., Mensah, A. A., Stengel, B., Drinovec, L., Mocnik, G., Zimmermann, R., Prévôt, A. S., and Gysel, M.: Brown and Black Carbon Emitted by a Marine Engine Operated on Heavy Fuel Oil and Distillate Fuels: Optical Properties, Size Distributions, and Emission Factors, Journal of Geophysical Research: Atmospheres, 123, 6175–6195, https://doi.org/10.1029/2017JD027818, 2018.

Dayan, U., Ricaud, P., Zbinden, R., and Dulac, F.: Atmospheric pollution over the eastern Mediterranean during summer–a review, Atmospheric Chemistry and Physics, 17, 13 233, 2017.

Di Biagio, C., Formenti, P., Cazaunau, M., Pangui, E., Marchand, N., and Doussin, J.-F.: Corrigendum to " Aethalometer multiple scattering correction C ref for mineral dust aerosols " published in Atmos . Meas . Tech ., 10 , 2923 – 2939 , 2017, Atmospheric Measurement Techniques, 10, 2923–2939, 2017.

Di Biagio, C., Formenti, P., Balkanski, Y., Caponi, L., Cazaunau, M., Pangui, E., Journet, E., Nowak, S., Andreae, M., Kandler, K., Saeed, T., Piketh, S., Seibert, D., Williams, E., and Doussin, J.-F.: Complex refractive indices and single scattering albedo of global dust aerosols in the shortwave spectrum and relationship to iron content and size, Complex refractive indices and single scattering albedo of global dust aerosols in the shortwave spectrum and relationship to iron content and size, pp. 1–42, https://doi.org/10.5194/acp-2019-145, 2019.

Drinovec, L., Močnik, G., Zotter, P., Prévôt, A., Ruckstuhl, C., Coz, E., Rupakheti, M., Sciare, J., Müller, T., Wiedensohler, A., and Hansen, A. D. A.: The "dual-spot" Aethalometer: an improved measurement of aerosol black carbon with real-time loading compensation, Atmospheric Measurement Techniques, 8, 1965–1979, 2015.

Drinovec, L., Gregoric, A., Zotter, P., Wolf, R., Anne Bruns, E., Bruns, E. A., Prevot, A. S., Favez, O., Sciare, J., Arnold, I. J., Chakrabarty, R. K., Moosmüller, H., Filep, A., and Mocnik, G.: The filter-loading effect by ambient aerosols in filter absorption photometers depends on the coating of the sampled particles, Atmospheric Measurement Techniques, 10, 1043–1059, https://doi.org/10.5194/amt-10-1043-2017, 2017.

Drinovec, L., Sciare, J., Stavroulas, I., Bezantakos, S., Pikridas, M., Unga, F., Savvides, C., Višić, B., Remškar, M., and Močnik, G.: A new optical-based technique for real-time measurements of mineral dust concentration in PM10 using a virtual impactor, Atmospheric Measurement Techniques Discussions, 2, 1–19, https://doi.org/10.5194/amt-2019-506, 2020.

Ealo, M., Alastuey, A., Ripoll, A., Pérez, N., Minguillón, M. C., Querol, X., and Pandolfi, M.: Detection of Saharan dust and biomass burning events using near-real-time intensive aerosol optical properties in the north-western Mediterranean, Atmospheric Chemistry and Physics, 16, 12 567–12 586, 2016.

Ealo, M., Alastuey, A., Pérez, N., Ripoll, A., Querol, X., and Pandolfi, M.: Impact of aerosol particle sources on optical properties in urban, regional and remote areas in the north-western Mediterranean., Atmospheric Chemistry & Physics, 18, 2018.

Escudero, M., Castillo, S., Querol, X., Avila, A., Alarcón, M., Viana, M. M., Alastuey, A., Cuevas, E., and Rodríguez, S.: Wet and dry African dust episodes over eastern Spain, Journal of Geophysical Research: Atmospheres, 110, https://doi.org/10.1029/2004JD004731, https://agupubs.onlinelibrary.wiley.com/doi/abs/10.1029/2004JD004731, 2005.

Ess, M. N. and Vasilatou, K.: Characterization of a new miniCAST with diffusion flame and premixed flame options: Generation of particles with high EC content in the size range 30 nm to 200 nm, Aerosol Science and Technology, 53, 29–44, https://doi.org/10.1080/02786826.2018.1536818, https://doi.org/10.1080/02786826.2018.1536818, 2019.

Ferrero, L., Ritter, C., Cappelletti, D., Moroni, B., Močnik, G., Mazzola, M., Lupi, A., Becagli, S., Traversi, R., Cataldi, M., Neuber, R., Vitale, V., and Bolzacchini, E.: Aerosol optical properties in the Arctic: The role of aerosol chemistry and dust composition in a closure experiment between Lidar and tethered balloon vertical profiles, Science of the Total Environment, 686, 452–467, https://doi.org/10.1016/j.scitotenv.2019.05.399, 2019.

Forello, A. C., Bernardoni, V., Calzolai, G., Lucarelli, F., Massabò, D., Nava, S., Pileci, R. E., Prati, P., Valentini, S., Valli, G., and Vecchi, R.: Exploiting multi-wavelength aerosol absorption coefficients in a multi-time source apportionment study to retrieve source-dependent absorption parameters, Atmospheric Chemistry and Physics Discussions, pp. 1–26, https://doi.org/10.5194/acp-2019-123, 2019.

Forello, A. C., Amato, F., Bernardoni, V., Calzolai, G., Canepari, S., Costabile, F., Di Liberto, L., Gualtieri, M., Lucarelli, F., Nava, S., Perrino, C., Petralia, E., Valentini, S., Valli, G., and Vecchi, R.: Gaining knowledge on source contribution to aerosol optical absorption

properties and organics by receptor modelling, Atmospheric Environment, 243, 117 873, https://doi.org/10.1016/j.atmosenv.2020.117873, https://doi.org/10.1016/j.atmosenv.2020.117873, 2020.

915 Freedman, D. and Diaconis, P.: On the histogram as a density estimator:L2 theory, Zeitschrift für Wahrscheinlichkeitstheorie und Verwandte Gebiete, 57, 453–476, https://doi.org/10.1007/BF01025868, 1981.

GAW: GAW Report No. 226: Coupled Chemistry-Meteorology/Climate Modelling (CCMM): status and relevance for numerical weather prediction, atmospheric pollution and climate research, WMO, 1172, 2016.

Gyawali, M., Arnott, W. P., Lewis, K., and Moosmüller, H.: In situ aerosol optics in Reno, NV, USA during and after the summer 2008 California wildfires and the influence of absorbing and non-absorbing organic coatings on spectral light absorption, Atmospheric Chemistry and Physics, 9, 8007–8015, https://doi.org/10.5194/acp-9-8007-2009, 2009.

Hansen, A., Rosen, H., and Novakov, T.: The aethaloemter- An instrument for the real-time measurement of optical absorption by particles, The Science of the Total Environment, 36, 191–196, 1984.

Houghton, J.T. Ding, Y. G. D. N. M. L. P. v. d. D. X. M. K. J. C.: Contribution of Working Group I to the Third Assessment Report of the
925 Intergovernmental Panel on Climate Change, Cambridge University Press, p. 94, 2001.

Kalivitis, N., Gerasopoulos, E., Vrekoussis, M., Kouvarakis, G., Kubilay, N., Hatzianastassiou, N., Vardavas, I., and Mihalopoulos, N.: Dust transport over the eastern Mediterranean derived from Total Ozone Mapping Spectrometer, Aerosol Robotic Network, and surface measurements, Journal of Geophysical Research: Atmospheres, 112, 2007.

Kirchstetter, T. W., Novakov, T., and Hobbs, P. V.: Evidence that the spectral dependence of light absorption by aerosols is affected by organic
930 carbon, Journal of Geophysical Research D: Atmospheres, 109, 1–12, https://doi.org/10.1029/2004JD004999, 2004a.

Kirchstetter, T. W., Novakov, T., and Hobbs, P. V.: Evidence that the spectral dependence of light absorption by aerosols is affected by organic carbon, Journal of Geophysical Research: Atmospheres, 109, 2004b.

Koçak, M., Mihalopoulos, N., and Kubilay, N.: Contributions of natural sources to high PM10 and PM2. 5 events in the eastern Mediterranean, Atmospheric Environment, 41, 3806–3818, 2007.

935 Lack, D. A., Lovejoy, E. R., Baynard, T., Pettersson, A., and Ravishankara, A. R.: Aerosol Absorption Measurement using Photoacoustic Spectroscopy: Sensitivity, Calibration, and Uncertainty Developments, Aerosol Science and Technology, 40, 697–708, https://doi.org/10.1080/02786820600803917, 2006.

Lack, D. A., Cappa, C. D., Covert, D. S., Baynard, T., Massoli, P., Sierau, B., Bates, T. S., Quinn, P. K., Lovejoy, E. R., and Ravishankara, A. R.: Bias in filter-based aerosol light absorption measurements due to organic aerosol loading: Evidence from ambient measurements,
940 Aerosol Science and Technology, 42, 1033–1041, https://doi.org/10.1080/02786820802389277, 2008.

Lack, D. A., Moosmüller, H., McMeeking, G. R., Chakrabarty, R. K., and Baumgardner, D.: Characterizing elemental, equivalent black, and refractory black carbon aerosol particles: A review of techniques, their limitations and uncertainties, Analytical and Bioanalytical Chemistry, 406, 99–122, https://doi.org/10.1007/s00216-013-7402-3, 2014.

Laing, J. R., Jaffe, D. A., and Sedlacek, A. J.: Comparison of filter-based absorption measurements of biomass burn-
945 ing aerosol and background aerosol at the mt. Bachelor observatory, Aerosol and Air Quality Research, 20, 663–678, https://doi.org/10.4209/aaqr.2019.06.0298, 2020.

Laj, P., Bigi, A., Rose, C., Andrews, E., Lund Myhre, C., Collaud Coen, M., Wiedensohler, A., Schultz, M., Ogren, J., Fiebig, M., Gliß, J., Mortier, A., Pandolfi, M., Petäjä, T., Kim, S.-W., Aas, W., Putaud, J.-P., Mayol-Bracero, O., Keywood, M., Labrador, L., Aalto, P., Ahlberg, E., Alados Arboledas, L., Alastuey, A., Andrade, M., Artíñano, B., Ausmeel, S., Arsov, T., Asmi, E., Backman, J., Baltensperger,
950 U., Bastian, S., Bath, O., Beukes, J. P., Brem, B., Bukowiecki, N., Conil, S., Couret, C., Day, D., Dayantolis, W., Degorska, A., Dos

Santos, S. M., Eleftheriadis, K., Fetfatzis, P., Favez, O., Flentje, H., Gini, M., Gregorič, A., Gysel-Beer, M., Hallar, G., Hand, J., Hoffer, A., Hueglin, C., Hooda, R., Hyvärinen, A., Kalapov, I., Kalivitis, N., Kasper-Giebl, A., Kim, J. E., Kouvarakis, G., Kranjc, I., Krejci, R., Kulmala, M., Labuschagne, C., Lee, H.-J., Lihavainen, H., Lin, N.-H., Löschau, G., Luoma, K., Marinoni, A., Meinhardt, F., Merkel, M., Metzger, J.-M., Mihalopoulos, N., Nguyen, N. A., Ondracek, J., Peréz, N., Perrone, M. R., Petit, J.-E., Picard, D., Pichon, J.-M., Pont, V., Prats, N., Prenni, A., Reisen, F., Romano, S., Sellegri, K., Sharma, S., Schauer, G., Sheridan, P., Sherman, J. P., Schütze, M., Schwerin, A., Sohmer, R., Sorribas, M., Steinbacher, M., Sun, J., Titos, G., Tokzko, B., Tuch, T., Tulet, P., Tunved, P., Vakkari, V., Velarde, F., Velasquez, P., Villani, P., Vratolis, S., Wang, S.-H., Weinhold, K., Weller, R., Yela, M., Yus-Diez, J., Zdimal, V., Zieger, P., and Zikova, N.: A global analysis of climate-relevant aerosol properties retrieved from the network of GAW near-surface observatories, Atmospheric Measurement Techniques, pp. 4353–4392, https://doi.org/10.5194/amt-13-4353-2020, 2020.

Laskin, A., Laskin, J., and Nizkorodov, S. A.: Chemistry of Atmospheric Brown Carbon, Chemical Reviews, 115, 4335–4382, https://doi.org/10.1021/cr5006167, 2015.

Lee, J. and Moosmüller, H.: Measurement of light absorbing aerosols with folded-jamin photothermal interferometry, Sensors (Switzerland), 20, 1–13, https://doi.org/10.3390/s20092615, 2020.

Lin, C. I., Baker, M., and Charlson, R. J.: Absorption Coefficient of Atmospheric Aerosol: a Method for Measurement., 1973.

Linke, C., Ibrahim, I., Schleicher, N., Hitzenberger, R., Andreae, M. O., Leisner, T., and Schnaiter, M.: A novel single-cavity three-wavelength photoacoustic spectrometer for atmospheric aerosol research, Atmospheric Measurement Techniques, 9, 5331–5346, https://doi.org/10.5194/amt-9-5331-2016, 2016.

Liousse, C., Cachier, H., and Jennings, S. G.: Optical and thermal measurements of black carbon aerosol content in different environments: Variation of the specific attenuation cross-section, sigma (σ), Atmospheric Environment Part A, General Topics, 27, 1203–1211, https://doi.org/10.1016/0960-1686(93)90246-U, 1993.

Liu, S., Aiken, A. C., Gorkowski, K., Dubey, M. K., Cappa, C. D., Williams, L. R., Herndon, S. C., Massoli, P., Fortner, E. C., Chhabra, P. S., Brooks, W. A., Onasch, T. B., Jayne, J. T., Worsnop, D. R., China, S., Sharma, N., Mazzoleni, C., Xu, L., Ng, N. L., Liu, D., Allan, J. D., Lee, J. D., Fleming, Z. L., Mohr, C., Zotter, P., Szidat, S., and Prévôt, A. S.: Enhanced light absorption by mixed source black and brown carbon particles in UK winter, Nature Communications, 6, https://doi.org/10.1038/ncomms9435, 2015.

Lyamani, H., Olmo, F., Alcántara, A., and Alados-Arboledas, L.: Atmospheric aerosols during the 2003 heat wave in southeastern Spain II: Microphysical columnar properties and radiative forcing, Atmospheric Environment, 40, 6465–6476, 2006.

Massabò, D., Bernardoni, V., Bove, M. C., Brunengo, A., Cuccia, E., Piazzalunga, A., Prati, P., Valli, G., and Vecchi, R.: A multi-wavelength optical set-up for the characterization of carbonaceous particulate matter, Journal of Aerosol Science, 60, 34–46, https://doi.org/10.1016/j.jaerosci.2013.02.006, 2013.

Mengis, N. and Matthews, H. D.: Non-CO2 forcing changes will likely decrease the remaining carbon budget for 1.5 °C, npj Climate and Atmospheric Science, 3, 1–7, https://doi.org/10.1038/s41612-020-0123-3, http://dx.doi.org/10.1038/s41612-020-0123-3, 2020.

Mona, L., Amodeo, A., Pandolfi, M., and Pappalardo, G.: Saharan dust intrusions in the Mediterranean area: Three years of Raman lidar measurements, Journal of Geophysical Research: Atmospheres, 111, 2006.

Moosmüller, H., Chakrabarty, R. K., and Arnott, W. P.: Aerosol light absorption and its measurement: A review, Journal of Quantitative Spectroscopy and Radiative Transfer, 110, 844–878, https://doi.org/10.1016/j.jqsrt.2009.02.035, 2009.

Müller, T.: Development of correction factors for Aethalometers AE31 and AE33, ACTRIS-2 WP3 Workshop, Athens, 10-12 November 2015, 2015.

Müller, T., Henzing, J., Leeuw, G. d., Wiedensohler, A., Alastuey, A., Angelov, H., Bizjak, M., Collaud Coen, M., Engström, J., Gruening, C., et al.: Characterization and intercomparison of aerosol absorption photometers: result of two intercomparison workshops, 2011a.

990 Müller, T., Laborde, M., Kassell, G., and Wiedensohler, A.: Design and performance of a three-wavelength LED-based total scatter and backscatter integrating nephelometer, Atmospheric Measurement Techniques, 4, 1291–1303, 2011b.

Myhre, G., Shindell, D., Breéon, F.-M., Collins, W., Fuglestvedt, J., Huang, J., Koch, D., Lamarque, J.-F., Lee, D., Mendoza, B., Nakajima, T., Robock, A., Stephens, G., Takemura, T., and Zhang, H.: Anthropogenic and Natural Radiative Forcing, book section 8, p. 659–740, Cambridge University Press, Cambridge, United Kingdom and New York, NY, USA, https://doi.org/10.1017/CBO9781107415324.018,

995 www.climatechange2013.org, 2013.

Ogren, J. A., Wendell, J., Andrews, E., and Sheridan, P. J.: Continuous light absorption photometer for long-Term studies, Atmospheric Measurement Techniques, 10, 4805–4818, https://doi.org/10.5194/amt-10-4805-2017, 2017.

Onasch, T. B., Massoli, P., Kebabian, P. L., Hills, F. B., Bacon, F. W., and Freedman, A.: Single scattering albedo monitor for airborne particulates, Aerosol Science and Technology, 49, 267–279, https://doi.org/10.1080/02786826.2015.1022248, 2015.

1000 Pandolfi, M., Cusack, M., Alastuey, A., and Querol, X.: Variability of aerosol optical properties in the Western Mediterranean Basin, Atmospheric Chemistry and Physics, 11, 8189–8203, 2011.

Pandolfi, M., Querol, X., Alastuey, A., Jimenez, J., Jorba, O., Day, D., Ortega, A., Cubison, M., Comerón, A., Sicard, M., et al.: Effects of sources and meteorology on particulate matter in the Western Mediterranean Basin: An overview of the DAURE campaign, Journal of Geophysical Research: Atmospheres, 119, 4978–5010, 2014a.

1005 Pandolfi, M., Ripoll, A., Querol, X., and Alastuey, A.: Climatology of aerosol optical properties and black carbon mass absorption cross section at a remote high-altitude site in the western Mediterranean Basin, Atmospheric Chemistry and Physics, 14, 6443–6460, 2014b.

Pandolfi, M., Tobias, A., Alastuey, A., Sunyer, J., Schwartz, J., Lorente, J., Pey, J., and Querol, X.: Effect of atmospheric mixing layer depth variations on urban air quality and daily mortality during Saharan dust outbreaks, Science of the Total Environment, 494, 283–289, 2014c.

Pandolfi, M., Alastuey, A., Pérez, N., Reche, C., Castro, I., Shatalov, V., and Querol, X.: Trends analysis of PM source contributions and

1010 chemical tracers in NE Spain during 2004–2014: a multi-exponential approach, Atmospheric Chemistry and Physics, 16, 11 787–11 805, 2016.

Pandolfi, M., Alados-Arboledas, L., Alastuey, A., Andrade, M., Angelov, C., Artiñano, B., Backman, J., Baltensperger, U., Bonasoni, P., Bukowiecki, N., Collaud Coen, M., Conil, S., Coz, E., Crenn, V., Dudoitis, V., Ealo, M., Eleftheriadis, K., Favez, O., Fetfatzis, P., Fiebig, M., Flentje, H., Ginot, P., Gysel, M., Henzing, B., Hoffer, A., Holubova Smejkalova, A., Kalapov, I., Kalivitis, N., Kouvarakis, G., Kris-

1015 tensson, A., Kulmala, M., Lihavainen, H., Lunder, C., Luoma, K., Lyamani, H., Marinoni, A., Mihalopoulos, N., Moerman, M., Nicolas, J., O'Dowd, C., Petäjä, T., Petit, J.-E., Pichon, J. M., Prokopciuk, N., Putaud, J.-P., Rodríguez, S., Sciare, J., Sellegri, K., Swietlicki, E., Titos, G., Tuch, T., Tunved, P., Ulevicius, V., Vaishya, A., Viana, M., Virkkula, A., Vratolis, S., Weingartner, E., Wiedensohler, A., and Laj, P.: A European aerosol phenomenology – 6: scattering properties of atmospheric aerosol particles from 28 ACTRIS sites, Atmospheric Chemistry and Physics, 18, 7877–7911, https://doi.org/10.5194/acp-18-7877-2018, https://www.atmos-chem-phys.net/18/7877/2018/, 2018.

1020 Park, S. S., Hansen, A. D., and Cho, S. Y.: Measurement of real time black carbon for investigating spot loading effects of Aethalometer data, Atmospheric Environment, 44, 1449–1455, https://doi.org/10.1016/j.atmosenv.2010.01.025, http://dx.doi.org/10.1016/j.atmosenv.2010.01.025, 2010.

Pérez, N., Pey, J., Castillo, S., Viana, M., Alastuey, A., and Querol, X.: Interpretation of the variability of levels of regional background aerosols in the Western Mediterranean, Science of the total environment, 407, 527–540, 2008.

Petzold, A. and Schönlinner, M.: Multi-angle absorption photometry—a new method for the measurement of aerosol light absorption and atmospheric black carbon, Journal of Aerosol Science, 35, 421–441, 2004.

Petzold, A., Schloesser, H., Sheridan, P. J., Arnott, W. P., Ogren, J. A., and Virkkula, A.: Evaluation of multiangle absorption photometry for measuring aerosol light absorption, Aerosol Science and Technology, 39, 40–51, https://doi.org/10.1080/027868290901945, 2005.

Petzold, A., Ogren, J. A., Fiebig, M., Laj, P., Li, S. M., Baltensperger, U., Holzer-Popp, T., Kinne, S., Pappalardo, G., Sugimoto, N., Wehrli, C., Wiedensohler, A., and Zhang, X. Y.: Recommendations for reporting black carbon measurements, Atmospheric Chemistry and Physics, 13, 8365–8379, https://doi.org/10.5194/acp-13-8365-2013, 2013.

Pey, J., Pérez, N., Castillo, S., Viana, M., Moreno, T., Pandolfi, M., López-Sebastián, J., Alastuey, A., and Querol, X.: Geochemistry of regional background aerosols in the Western Mediterranean, Atmospheric Research, 94, 422–435, 2009.

Pey, J., Querol, X., Alastuey, A., Forastiere, F., and Stafoggia, M.: African dust outbreaks over the Mediterranean Basin during 2001–2011: PM 10 concentrations, phenomenology and trends, and its relation with synoptic and mesoscale meteorology, Atmospheric Chemistry and Physics, 13, 1395–1410, 2013.

Querol, X., Alastuey, A., Puicercus, J. A., Mantilla, E., Miro, J. V., Lopez-Soler, A., Plana, F., and Artiñano, B.: Seasonal evolution of suspended particles around a large coal-fired power station: particulate levels and sources, Atmospheric Environment, 32, 1963–1978, 1998.

Querol, X., Alastuey, A., Rodriguez, S., Plana, F., Ruiz, C. R., Cots, N., Massagué, G., and Puig, O.: PM10 and PM2. 5 source apportionment in the Barcelona Metropolitan area, Catalonia, Spain, Atmospheric Environment, 35, 6407–6419, 2001.

Querol, X., Alastuey, A., Viana, M. M., Rodriguez, S., Artíñano, B., Salvador, P., Do Santos, S. G., Fernandez Patier, R., Ruiz, C., De la Rosa, J., Sanchez de la Campa, A., Menendez, M., and Gil, J.: Speciation and origin of PM10 and PM2. 5 in Spain, Journal of Aerosol Science, 35, 1151–1172, 2004.

Querol, X., Alastuey, A., Pey, J., Cusack, M., Pérez, N., Mihalopoulos, N., Theodosi, C., Gerasopoulos, E., Kubilay, N., and Koçak, M.: Variability in regional background aerosols within the Mediterranean., Atmospheric Chemistry & Physics Discussions, 9, 2009a.

Querol, X., Pey, J., Pandolfi, M., Alastuey, A., Cusack, M., Pérez, N., Moreno, T., Viana, M., Mihalopoulos, N., Kallos, G., et al.: African dust contributions to mean ambient PM10 mass-levels across the Mediterranean Basin, Atmospheric Environment, 43, 4266–4277, 2009b.

Querol, X., Perez, N., Reche, C., Ealo, M., Ripoll, A., Tur, J., Pandolfi, M., Pey, J., Salvador, P., Moreno, T., et al.: African dust and air quality over Spain: Is it only dust that matters?, Science of the total environment, 686, 737–752, 2019.

Ramanathan, V. and Carmichael, G.: Global and regional climate changes due to black carbon, Nature Geoscience, 1, 221–227, https://doi.org/10.1038/ngeo156, 2008.

Ramanathan, V., Crutzen, P., Kiehl, J., and Rosenfeld, D.: Aerosols, climate, and the hydrological cycle, science, 294, 2119–2124, 2001.

Reche, C., Querol, X., Alastuey, A., Viana, M., Pey, J., Moreno, T., Rodríguez, S., González, Y., Fernández-Camacho, R., Rosa, J., et al.: New considerations for PM, Black Carbon and particle number concentration for air quality monitoring across different European cities, Atmospheric Chemistry and Physics, 11, 6207–6227, 2011.

Rigler, M., Drinovec, L., Lavri, G., Vlachou, A., Prevot, A. S., Luc Jaffrezo, J., Stavroulas, I., Sciare, J., Burger, J., Kranjc, I., Turšič, J., D. A. Hansen, A., and Mocnik, G.: The new instrument using a TC-BC (total carbon-black carbon) method for the online measurement of carbonaceous aerosols, Atmospheric Measurement Techniques, 13, 4333–4351, https://doi.org/10.5194/amt-13-4333-2020, 2020.

Ripoll, A., Pey, J., Minguillón, M. C., Pérez, N., Pandolfi, M., Querol, X., and Alastuey, A.: Three years of aerosol mass, black carbon and particle number concentrations at Montsec (southern Pyrenees, 1570 m asl), Atmospheric Chemistry and Physics, 14, 4279–4295, 2014.

Ripoll, A., Minguillón, M. C., Pey, J., Jimenez, J. L., Day, D. A., Sosedova, Y., Canonaco, F., Prévôt, A. S., Querol, X., and Alastuey, A.: Long-term real-time chemical characterization of submicron aerosols at Montsec (southern Pyrenees, 1570 m a.s.l.), Atmospheric Chemistry and Physics, 15, 2935–2951, https://doi.org/10.5194/acp-15-2935-2015, 2015.

1065 Rivas, I., Beddows, D. C., Amato, F., Green, D. C., Järvi, L., Hueglin, C., Reche, C., Timonen, H., Fuller, G. W., Niemi, J. V., et al.: Source apportionment of particle number size distribution in urban background and traffic stations in four European cities, Environment International, 135, 105 345, 2020.

Rodrıguez, S., Querol, X., Alastuey, A., Kallos, G., and Kakaliagou, O.: Saharan dust contributions to PM10 and TSP levels in Southern and Eastern Spain, Atmospheric Environment, 35, 2433–2447, 2001.

1070 Rodríguez, S., Querol, X., Alastuey, A., and Plana, F.: Sources and processes affecting levels and composition of atmospheric aerosol in the western Mediterranean, Journal of Geophysical Research: Atmospheres, 107, AAC–12, 2002.

Samset, B. H., Sand, M., Smith, C. J., Bauer, S. E., Forster, P. M., Fuglestvedt, J. S., Osprey, S., and Schleussner, C. F.: Climate Impacts From a Removal of Anthropogenic Aerosol Emissions, Geophysical Research Letters, 45, 1020–1029, https://doi.org/10.1002/2017GL076079, 2018.

1075 Sandradewi, J., Prévôt, A. S., Szidat, S., Perron, N., Alfarra, M. R., Lanz, V. A., Weingartner, E., and Baltensperger, U. R.: Using aerosol light absorption measurements for the quantitative determination of wood burning and traffic emission contribution to particulate matter, Environmental Science and Technology, 42, 3316–3323, https://doi.org/10.1021/es702253m, 2008.

Schauer, G., Kasper-Giebl, A., and Močnik, G.: Increased PM concentrations during a combined wildfire and saharan dust event observed at high-altitude Sonnblick observatory, Austria, Aerosol and Air Quality Research, 16, 542–554, https://doi.org/10.4209/aaqr.2015.05.0337,

1080 2016.

Schmeisser, L., Backman, J., Ogren, J. A., Andrews, E., Asmi, E., Starkweather, S., Uttal, T., Fiebig, M., Sharma, S., Eleftheriadis, K., Vratolis, S., Bergin, M., Tunved, P., and Jefferson, A.: Seasonality of aerosol optical properties in the Arctic, Atmospheric Chemistry and Physics, 18, 11 599–11 622, https://doi.org/10.5194/acp-18-11599-2018, 2018.

Schmid, O., Artaxo, P., Arnott, W. P., Chand, D., Gatti, L. V., Frank, G. P., Hoffer, A., Schnaiter, M., and Andreae, M. O.: Spectral light

1085 absorption by ambient aerosols influenced by biomass burning in the Amazon Basin. I: Comparison and field calibration of absorption measurement techniques, Atmospheric Chemistry and Physics, 6, 3443–3462, https://doi.org/10.5194/acp-6-3443-2006, 2006.

Segura, S., Estellés, V., Titos, G., Lyamani, H., Utrillas, M. P., Zotter, P., Prévôt, A. S., Močnik, G., Alados-Arboledas, L., and Martínez-Lozano, J. A.: Determination and analysis of in situ spectral aerosol optical properties by a multi-instrumental approach, Atmospheric Measurement Techniques, 7, 2373–2387, https://doi.org/10.5194/amt-7-2373-2014, 2014.

1090 Sheridan, P. J., Patrick Arnott, W., Ogren, J. A., Andrews, E., Atkinson, D. B., Covert, D. S., Moosmüller, H., Petzold, A., Schmid, B., Strawa, A. W., Varma, R., and Virkkula, A.: The reno aerosol optics study: An evaluation of aerosol absorption measurement methods, Aerosol Science and Technology, 39, 1–16, https://doi.org/10.1080/027868290901891, 2005.

Singh, S., Fiddler, M. N., Smith, D., and Bililign, S.: Error analysis and uncertainty in the determination of aerosol optical properties using cavity ring-down spectroscopy, integrating nephelometry, and the extinction-minus-scattering method, Aerosol Science and Technology,

1095 48, 1345–1359, https://doi.org/10.1080/02786826.2014.984062, 2014.

Sokolik, I. N. and Toon, O. B.: Incorporation of mineralogical composition into models of the radiative properties of mineral aerosol from UV to IR wavelengths, Journal of Geophysical Research Atmospheres, 104, 9423–9444, https://doi.org/10.1029/1998JD200048, 1999.

Springston, S. R. and Sedlacek, A. J.: Noise characteristics of an instrumental particle absorbance technique, Aerosol Science and Technology, 41, 1110–1116, https://doi.org/10.1080/02786820701777457, 2007.

Stephens, M., Turner, N., and Sandberg, J.: Particle identification by laser-induced incandescence in a solid-state laser cavity, Applied Optics, 42, 3726, https://doi.org/10.1364/ao.42.003726, 2003.

Terhune, R. W. and Anderson, J. E.: Spectrophone measurements of the absorption of visible light by aerosols in the atmosphere, Optics Letters, 1, 70, https://doi.org/10.1364/ol.1.000070, 1977.

Valentini, S., Barnaba, F., Bernardoni, V., Calzolai, G., Costabile, F., Di Liberto, L., Forello, A. C., Gobbi, G. P., Gualtieri, M., Lucarelli, F., Nava, S., Petralia, E., Valli, G., Wiedensohler, A., and Vecchi, R.: Classifying aerosol particles through the combination of optical and physical-chemical properties: Results from a wintertime campaign in Rome (Italy), Atmospheric Research, 235, 104 799, https://doi.org/10.1016/j.atmosres.2019.104799, https://doi.org/10.1016/j.atmosres.2019.104799, 2020a.

Valentini, S., Bernardoni, V., Bolzacchini, E., Ciniglia, D., Pandolfi, M., Ferrero, L., Forello, A. C., Massabó, D., Pandolfi, M., Prati, P., Soldan, F., Valli, G., Yus-díez, J., and Vecchi, R.: Applicability of benchtop multi-wavelength polar photometers to off-line measurements of the Multi-Angle Absorption Photometer, pp. 1–13, https://doi.org/10.1016/j.jaerosci.2020.105701, 2020b.

Vecchi, R., Bernardoni, V., Paganelli, C., and Valli, G.: A filter-based light-absorption measurement with polar photometer: Effects of sampling artefacts from organic carbon, Journal of Aerosol Science, 70, 15–25, 2014.

Virkkula, A., Mäkelä, T., Hillamo, R., Yli-Tuomi, T., Hirsikko, A., Hämeri, K., and Koponen, I. K.: A simple procedure for correcting loading effects of aethalometer data, Journal of the Air and Waste Management Association, 57, 1214–1222, https://doi.org/10.3155/1047-3289.57.10.1214, 2007.

Virkkula, A., Chi, X., Ding, A., Shen, Y., Nie, W., Qi, X., Zheng, L., Huang, X., Xie, Y., Wang, J., Petäjä, T., and Kulmala, M.: On the interpretation of the loading correction of the aethalometer, Atmospheric Measurement Techniques, 8, 4415–4427, https://doi.org/10.5194/amt-8-4415-2015, 2015.

Visser, B., Röhrbein, J., Steigmeier, P., Drinovec, L., Močnik, G., and Weingartner, E.: A single-beam photothermal interferometer for in-situ measurements of aerosol light absorption, Atmospheric Measurement Techniques Discussions, 2, 1–24, https://doi.org/10.5194/amt-2020-242, 2020.

Wang, Y., Le, T., Chen, G., Yung, Y. L., Su, H., Seinfeld, J. H., and Jiang, J. H.: Reduced European aerosol emissions suppress winter extremes over northern Eurasia, Nature Climate Change, 10, 225–230, https://doi.org/10.1038/s41558-020-0693-4, http://dx.doi.org/10.1038/s41558-020-0693-4, 2020.

Weingartner, E., Saathoff, H., Schnaiter, M., Streit, N., Bitnar, B., and Baltensperger, U.: Absorption of light by soot particles: Determination of the absorption coefficient by means of aethalometers, Journal of Aerosol Science, 34, 1445–1463, https://doi.org/10.1016/S0021-8502(03)00359-8, 2003.

WMO: WMO/GAW Aerosol Measurement Procedures, Guidelines and Recommendations, WMO- No. 1177; GAW Report- No. 227, https://library.wmo.int/doc{_}num.php?explnum{_}id=3073, 2016.

Yus-Díez, J., Ealo, M., Pandolfi, M., Perez, N., Titos, G., Močnik, G., Querol, X., and Alastuey, A.: Aircraft vertical profiles during summertime regional and Saharan dust scenarios over the north-western Mediterranean Basin: aerosol optical and physical properties, Atmospheric Chemistry and Physics Discussions, pp. 1–35, 2020.

Zanatta, M., Gysel, M., Bukowiecki, N., Müller, T., Weingartner, E., Areskoug, H., Fiebig, M., Yttri, K. E., Mihalopoulos, N., Kouvarakis, G., et al.: A European aerosol phenomenology-5: Climatology of black carbon optical properties at 9 regional background sites across Europe, Atmospheric environment, 145, 346–364, 2016.

Zhang, Y., Favez, O., Canonaco, F., Liu, D., Močnik, G., Amodeo, T., Sciare, J., Prévôt, A. S. H., Gros, V., and Albinet, A.: Evidence of major secondary organic aerosol contribution to lensing effect black carbon absorption enhancement, npj Climate and Atmospheric Science, 1, https://doi.org/10.1038/s41612-018-0056-2, 2018.

Zotter, P., Herich, H., Gysel, M., El-Haddad, I., Zhang, Y., Mocnik, G., Hüglin, C., Baltensperger, U., Szidat, S., and Prévôt, A. S.: Evaluation of the absorption Ångström exponents for traffic and wood burning in the Aethalometer-based source apportionment using radiocarbon measurements of ambient aerosol, Atmospheric Chemistry and Physics, 17, 4229–4249, https://doi.org/10.5194/acp-17-4229-2017, 2017.